Yanbu Journal of Engineering and Science

Volume 23 | Issue 1 Article 8

2026

CFD-Based Thermal Performance Analysis of Dimpled and Grooved Heat Pipes

Mazen M. Othayq
Department of Mechanical Engineering, College of Engineering and Computer Sciences, Jazan University, Jazan 45142, Saudi Arabia AND Engineering and Technology Research Center, Jazan University, P.O. Box 114, Jazan, 82817, Saudi Arabia, Mothayq@jazanu.edu.sa

Khalid M. Alanazi
Department of Mechanical Engineering, Faculty of Engineering, University of Tabuk, Tabuk 71491, Saudi Arabia

Follow this and additional works at: https://yjes.researchcommons.org/yjes

The journal in which this article appears is hosted on Digital Commons, an Elsevier platform.

Recommended Citation

Othayq, Mazen M. and Alanazi, Khalid M. (2026), CFD-Based Thermal Performance Analysis of Dimpled and Grooved Heat Pipes, *Yanbu Journal of Engineering and Science*: Vol. 23: Iss. 1, 119-141.
DOI: https://doi.org/10.53370/3122-3303.1214
Available at: https://yjes.researchcommons.org/yjes/vol23/iss1/8

This Research Article is brought to you for free and open access by Yanbu Journal of Engineering and Science. It has been accepted for inclusion in Yanbu Journal of Engineering and Science by an authorized editor of Yanbu Journal of Engineering and Science.

YANBU JOURNAL OF ENGINEERING AND SCIENCE 2026;23:119–141

Scan the QR to view the full-text article on the journal website

RESEARCH ARTICLE

CFD-Based Thermal Performance Analysis of Dimpled and Grooved Heat Pipes

Mazen M. Othayq [a,b,*], **Khalid M. Alanazi** [c]

[a] Department of Mechanical Engineering, College of Engineering and Computer Sciences, Jazan University, Jazan 45142, Saudi Arabia
[b] Engineering and Technology Research Center, Jazan University, P.O. Box 114, Jazan, 82817, Saudi Arabia
[c] Department of Mechanical Engineering, Faculty of Engineering, University of Tabuk, Tabuk 71491, Saudi Arabia

ABSTRACT

Heat-transfer enhancement techniques such as fins, dimples, and grooves are widely employed to improve the thermal performance of heat exchangers; however, their application is often accompanied by increased pressure losses. Most existing studies investigate a single enhancement technique over a limited Reynolds number range, with few comparative analyses conducted at high Reynolds numbers using identical geometries. Therefore, this study numerically investigates the thermal–hydraulic performance of five pipe configurations using Computational Fluid Dynamics (CFD). All geometries share the same diameter (48.34 mm) and length (7.45 m) and are examined over a Reynolds number range of 4,000–57,000. The configurations include: (1) smooth pipe, (2) pipe with spherical convex dimples, (3) pipe with spherical concave dimples, (4) pipe with circumferential grooves of depth (e) to diameter (d) ratio of 0.20, and (5) pipe with circumferential grooves of $e/d = 0.50$. A mesh-independence study was performed for both smooth and dimpled pipes, followed by CFD validation against available experimental data and empirical correlations from three different sources in the literature. After validation, local temperature, pressure, and velocity fields were analyzed at the highest flow Reynolds number ($Re = 57{,}000$). In addition, the effects of Reynolds number on Nusselt number, friction factor, and thermal performance factor (TPF) were evaluated for each pipe case. Results indicate that dimples and grooves promote recirculation and near-wall mixing, enhancing heat transfer relative to the smooth pipe. The groove configuration with $e/d = 0.50$ achieved the highest TPF ($\approx$1.45 at $Re = 57{,}000$), but with a 456% increase in friction factor. Whereas the $e/d = 0.20$ case provided a more balanced thermal–hydraulic performance.

Keywords: CFD, Heat transfer enhancement, Dimpled pipe, Grooved pipe, Thermal performance analysis

1. Introduction

Pipes are used in various thermal engineering applications, such as heat exchangers in power plants, heating, ventilating, and air conditioning (HVAC) systems [1]. In these systems, thermal energy is transferred between two or more fluids by conduction through the pipe wall and by forced convection within the pipe core. Enhancing this heat-transfer process through surface modification of the pipe wall has attracted significant attention within the scientific community. Certain geometric modifications can substantially improve heat transfer by increasing the effective heat-transfer area, disrupting and thinning thermal boundary layers, and intensifying momentum and energy exchange between the wall and the flowing fluid.

Unlike smooth pipe walls, heat exchangers incorporating surface roughness elements—such as dimples, grooves, turbulators, and protrusions—exhibit superior thermo-hydraulic performance due to enhanced fluid mixing, stronger eddy formation, and controlled flow separation [2, 3]. These mechanisms lead to higher convective heat-transfer coefficients and reduced thermal resistance at the wall–fluid interface [4, 5]. However, such improvements are inevitably

Received 29 November 2025; revised 26 February 2026; accepted 12 April 2026.
Available online 29 April 2026

* Corresponding author.
E-mail addresses: Mothayq@jazanu.edu.sa (M. M. Othayq), Kalshmlani@ut.edu.sa (K. M. Alanazi).

https://doi.org/10.53370/3122-3303.1214
3122-3303/© 2026 The Author(s). Yanbu Journal of Engineering and Science. This is an open access article under the CC BY 4.0 Licence (https://creativecommons.org/licenses/by/4.0/).
Published by Yanbu Industrial College, Saudi Arabia. The journal is hosted on Digital Commons, an Elsevier Platform.

Latin Symbol			
A	Heat transfer area, m^2	C_p	Specific heat, $J{\cdot}kg^{-1}{\cdot}K^{-1}$
d	Dimple or Groove diameter, m	D_h	Hydraulic diameter, m
e	Dimple or Groove depth, m	fr	Darcy friction factor, -
h_{ave}	Avg. Conv. heat transfer coeff., $W{\cdot}m^{-2}{\cdot}K^{-1}$	k	Thermal conductivity, $W{\cdot}m^{-1}{\cdot}K^{-1}$
L	Pipe length, m	Nu	Nusselt number, -
P	Dimple or groove pitch, m	ΔP	Pressure drop, Pa
q''	Applied wall heat flux, $W{\cdot}m^{-2}$	r	Radial distance from pipe center, m
Re	Reynolds number, -	T	Temperature, K or °C
u_i	Velocity component in (i)-direction, $m{\cdot}s^{-1}$	U	Mean bulk-fluid velocity, $m{\cdot}s^{-1}$
x_i	Spatial coordinate in (i)-direction, m	L	Pipe length, m
$\dot{m}$	Mass flow rate, $kg{\cdot}s^{-1}$	u_i	Mean velocity in (i)-direction, $m{\cdot}s^{-1}$
T_{in}	Fluid temperature at inlet, K or °C	T_{out}	Fluid temperature at outlet, K or °C
T_b	Fluid bulk temperature, K or °C	T_w	Pipe wall temperature, K or °C
Greek Symbols			
α	Thermal diffusivity, $m^2{\cdot}s^{-1}$	μ	Dynamic viscosity, $kg{\cdot}m^{-1}{\cdot}s^{-1}$
ν	Kinematic viscosity, $m^2{\cdot}s^{-1}$	ν_t	Turbulent eddy viscosity
ρ	Fluid density, $kg{\cdot}m^{-3}$	$ui'uj'$	Reynolds stress tensor, $m^{-2}{\cdot}s^{-2}$
Subscripts			
b	Bulk (mean fluid value)	exp	Experimental
f	Fluid	(i, j)	Spatial indices
in	Inlet	out	Outlet
w	wall		
Superscripts			
$\bar{}$	Reynolds-averaged quantity	$'$	fluctuating component
Abbreviations			
CFD	Computational Fluid Dynamics	SIMPLEC	Semi-Implicit Method for Pressure-Linked Equations–Consistent
RANS	Reynolds-Averaged Navier-Stokes		
RSM	Reynolds Stress Model	PRESTO	Pressure Staggering Option
ANSYS	Analysis System	k-ε or k-ω	Specific Kinetic energy and dissipate rates models

accompanied by increased pressure drop [6, 7], requiring careful thermo-hydraulic optimization to ensure overall performance enhancement. Previous studies [8–12] consistently report that these surface features significantly improve the heat-transfer performance of tube heat exchangers compared with conventional smooth tubes, primarily due to their ability to promote near-wall turbulence and periodic boundary-layer reattachment.

Several studies [13–18] have shown that introducing geometric irregularities into smooth pipes significantly modifies near-wall flow structures and thermal boundary-layer development. Such features generate recirculation zones and periodic flow separation and reattachment, increasing turbulence intensity and local shear stress [19]. As a result, the thermal boundary layer is repeatedly disrupted, enhancing convective heat transfer but also increasing frictional losses. For dimpled surfaces, key geometric parameters strongly influence thermo-hydraulic performance. Dimple diameter controls the size and strength of recirculation zones [13, 15, 20], dimple shape governs vortex formation and downstream impingement behavior [10, 14, 21–25], and pitch determines the interaction between successive disturbed flow regions [13, 26]. Collectively, these parameters dictate the balance between heat-transfer enhancement and pressure-drop penalty.

Al-Obaidi and Chaer [18] numerically investigated inserted turbulator balls with diameters ranging from 1 mm to 8 mm and reported that the largest diameter (8 mm) generated the highest turbulent kinetic energy, leading to improved thermal performance. Similarly, Al-Obaidi and Alhamid [15] examined spherical dimples with diameters between 1 mm and 4 mm in an 11.08 mm diameter pipe and found that

the largest dimples (4 mm) produced the strongest recirculation and fluid mixing, resulting in the greatest heat-transfer enhancement.

Extending the analysis to dimple shape, Ali et al. [14] numerically examined square, circular, and triangular dimples on an aluminum pipe ($D = 0.03$ m) under a uniform heat flux of 40 kW/m^2 and Reynolds numbers between 3,500 and 7,000. Although all shapes enhanced heat transfer relative to a smooth pipe, they also increased friction losses. Triangular dimples produced the highest pressure drop, whereas circular dimples achieved the most favorable overall thermal performance. Similarly, Zhou and Acharya [23] performed combined experimental and numerical investigations of triangular, circular, square, and teardrop-shaped dimples in a square channel at $Re = 21,000$, reporting that teardrop dimples provided the greatest heat-transfer enhancement due to more effective vortex formation and reduced flow-separation penalties.

In addition to size and shape, geometric spacing and depth have been shown to play a critical role in thermo-hydraulic performance. Xie et al. [27] numerically examined the effects of radius, pitch, and depth in pipes with dimples and protrusions and concluded that pitch and depth exerted a stronger influence on heat-transfer enhancement than radius. Similarly, Ali and Shehab [11] investigated the effects of dimple arrangement, diameter, and orientation in a double pipe heat exchanger and reported that, for Reynolds numbers between 5,000 and 20,000, staggered configurations at 60° and 90° significantly intensified flow disturbance. These arrangements increased the Nusselt number by 7.55–11.2 times relative to smooth pipes and improved thermal performance by approximately 50% compared with in-line configurations, highlighting the importance of geometric optimization in dimpled heat-transfer surfaces.

Various tube configurations incorporating ribs and corrugations have also demonstrated substantial improvements in heat-transfer performance by intensifying flow disturbance and sustaining turbulence along the heat-transfer surface. Naphon et al. [28] experimentally investigated twin tubes with helical ribs of varying height-to-diameter and pitch-to-diameter ratios and attributed the observed enhancement to strong secondary flows induced by the ribbed geometry. Similarly, Laohalertdecha and Wongwises [29] studied condensation heat transfer of R-134a in a horizontal corrugated aluminum tube and reported up to a 70% increase in the heat-transfer coefficient compared with a smooth tube for Reynolds numbers between 6,000 and 27,000. Pethkool et al. [30] examined helically corrugated tubes and observed heat-transfer enhancements of up to 232%, accompanied by corresponding increases in friction factor and Nusselt number, underscoring the trade-off between thermal augmentation and pressure-drop penalty.

Similar trends were reported by Elshafei et al. [31] in corrugated channels, where heat transfer and pressure drop increased by up to 3.2 and 2.6 times, respectively. Extending these results to a wider operating range, Dong et al. [32] demonstrated the effectiveness of corrugated geometries for water flow at Reynolds numbers between 6,000 and 93,000, achieving heat-transfer enhancements of up to 160%. Collectively, these findings confirm that ribs and corrugations effectively augment convective heat transfer by promoting enhanced mixing and secondary flow formation. However, the associated increase in frictional losses necessitates careful thermo-hydraulic optimization to ensure overall performance improvement.

Talib et al. [33] further examined the coupled effects of flow regime and surface geometry by investigating rib pitch-to-diameter ratios (P/D = 1.3, 1.5, 1.8) in helical ribbed rectangular tubes. At relatively low Reynolds numbers ($Re \approx 10,000$), variations in rib configuration produced only modest differences in Nusselt number (≈ 70) and friction factor (≈ 0.005). However, as the Reynolds number increased to 30,000, these differences more than doubled, indicating that the influence of surface irregularities becomes more pronounced under stronger turbulent conditions. These observations align with the findings of Al-Obaidi and Alhamid [15] and Leontiev et al. [34], who emphasized that thermal enhancement depends not only on geometric design but also on its interaction with the prevailing flow regime.

Further evidence of the dominant role of flow characteristics was provided by Jackson et al. [35], who examined the thermal response of a heat pipe under both transient (ramp-up) and steady-state conditions. The water mass flow rate was increased from 0.28 to 2.28 kg/s over ramp-up periods of 3–60 s, while maintaining a constant wall heat flux of 8,800 W/m^2. The results showed a clear and monotonic decrease in both local fluid and wall temperatures with increasing flow rate, demonstrating the strong sensitivity of heat-transfer behavior to transient flow dynamics. These findings further emphasize that optimal thermal performance in heat exchangers and heat pipes depends on the interplay between surface geometry and flow regime, underscoring the fundamental thermo-hydraulic coupling governing convective heat-transfer enhancement.

The coupled interaction between flow conditions and surface irregularities—such as dimples and protrusions—has led to inconsistent conclusions regarding their influence on heat-transfer enhancement

and flow structure. Duo et al. [36], for example, examined the effect of dimple location in a pin-finned channel and reported only a modest Nusselt number (*Nu*) increase of 3.52% when dimples were placed within the wake region relative to a smooth channel. However, relocating the dimples away from the wake region resulted in a substantially higher *Nu* enhancement of up to 20.94%. Meanwhile, the friction coefficient slightly decreased, from 1.82% to 1.69%, as the dimples were positioned outside the wake region, illustrating the sensitivity of thermo-hydraulic performance to geometric placement within the flow field.

Similarly, Fan et al. [37] investigated ellipse-shaped dimples on a finned-tube heat exchanger and reported significant increases in both the Nusselt number and friction coefficient. Under identical flow conditions, the dimpled configuration enhanced heat transfer by approximately 13.8–30.3% compared with a plain finned-tube heat exchanger. In addition, Katkhaw et al. [38] examined 45° ellipsoidal dimples on flat plates and observed that a staggered arrangement increased the heat-transfer coefficient by 15.8% relative to a smooth plate, while an inline configuration yielded an even greater Nusselt number enhancement of 21.7%.

In contrast, Piper et al. [39], investigated pillow-plate heat exchangers and reported only marginal heat-transfer enhancement—no more than 2.2%—following the introduction of dimples. These discrepancies indicate that a definitive assessment of dimple effectiveness remains unresolved. Their performance appears to be strongly governed by the complex interaction among flow conditions, geometric configuration, dimple arrangement and placement, and other surface characteristics, highlighting the need for further systematic investigation.

Farsad et al. [40] numerically investigated fluid-flow mechanisms and heat-transfer characteristics in a 15 mm diameter pipe with dimples and protrusions using a CFD approach. Their results showed that vortices formed near the wall within the dimple and protrusion cavities, enhancing flow mixing and promoting more effective wall–fluid heat exchange. Consequently, the convective heat-transfer coefficient increased by 36.21% compared with a smooth pipe at $Re = 12{,}000$.

Recently, Al-Haidari et al. [41] numerically and experimentally investigated the effects of dimple shape and number on heat-transfer enhancement in a 23 mm diameter pipe using water as the working fluid over Reynolds numbers ranging from 4,000 to 15,000. The examined geometries included cylindrical, spherical, and polygonal dimples, with 3, 4, and 5 dimples for each shape. All configurations enhanced heat transfer compared with a smooth pipe. Among the shapes, spherical dimples achieved the highest Performance Evaluation Factor (PEF) of 1.408, while the PEF for cylindrical and polygonal dimples was lower by 8.3% and 5.6%, respectively. Increasing the number of cylindrical and polygonal dimples to five improved heat transfer but also led to higher pressure drop and friction factor. In contrast, the configuration with three dimples yielded the highest overall PEF, indicating a more favorable thermo-hydraulic balance.

Despite the extensive literature on heat-transfer enhancement using surface irregularities such as dimples, ribs, and corrugations, important gaps remain. Most previous studies have evaluated individual enhancement techniques in isolation, with limited direct comparison of different tube geometries under identical operating conditions, particularly at high Reynolds numbers. Moreover, the underlying flow and thermal mechanisms—such as recirculation, near-wall mixing, and pressure-gradient effects—are often examined over short tube lengths that may not reflect practical heat-exchanger behavior. Accordingly, a systematic and comparative assessment of multiple tube geometries under consistent boundary conditions is still lacking. The present study addresses this gap by evaluating different surface configurations at high Reynolds numbers to clarify the coupled influence of surface geometry and flow regime on overall thermo-hydraulic performance.

To address this gap, the present study numerically investigates the thermo-hydraulic performance of five pipe configurations using a validated Computational Fluid Dynamics (CFD) approach: (1) a smooth pipe, (2) a pipe with spherical convex dimples, (3) a pipe with concave spherical dimples, (4) a pipe with circumferential grooves of normalized depth-to-diameter ratio ($e/d = 0.20$), and (5) a pipe with deeper grooves ($e/d = 0.50$). The CFD model for the smooth pipe was first validated against experimental temperature data from the literature [35]. In addition, the surface-modified pipe with dimples was validated with available experimental data that was adopted from Al-Haidari et al. [41]. After validation, simulations of the modified geometries were conducted under identical boundary conditions over a Reynolds number range of 30,000–57,000. Heat-transfer performance was evaluated in terms of Nusselt number, friction factor, and thermal performance factor (TPF), with comparisons made relative to the smooth pipe baseline. This systematic analysis aims to clarify the coupled influence of surface geometry and high-Reynolds-number flow on overall thermo-hydraulic performance.

2. Materials and methods

The numerical methodology in this study comprises three main stages: (i) geometry creation, (ii) mesh generation, and (iii) CFD simulation of the working fluid in the pipes investigated using ANSYS Fluent. Each stage is described in detail in the following subsections.

2.1. Pipe geometry

Five circular heat pipes were modeled in SolidWorks 2024, as shown in Fig. 1. The configurations include: (a) smooth pipe, (b) spherical convex dimples, (c) spherical concave dimples, (d) circumferential grooves with $e/d = 0.20$, and (e) grooves with $e/d = 0.50$. Here, d, e/d, and P/d denote the dimple diameter, depth-to-diameter ratio, and pitch-to-diameter ratio, respectively. All pipes have the same inner diameter (48.34 mm) and length (7.45 m). For the dimpled cases, the diameter and pitch were fixed at 0.010 m and 0.050 m, with six features uniformly spaced (60° apart) along the circumference. A constant $P/d = 5$ was used, except for the grooved pipe with $e/d = 0.20$ ($P/d = 3$). It is worth noting that the dimensionless ratios, e/d and P/d, considered in this work fall within the ranges reported in the literature [42].

2.2. Governing equations

2.2.1. Steady-state equations for turbulent incompressible flow

In the present study, the flow is highly turbulent and was analyzed using a steady-state approach. The turbulence was modeled employing the Reynolds Stress Model (RSM) in conjunction with an enhanced wall treatment. For turbulent incompressible flow under steady-state conditions, the continuity equation—expressed in indicial notation using Reynolds-averaged quantities—can be written as follows:

$$\frac{\partial \bar{u}_i}{\partial x_i} = 0, \tag{1}$$

where $\bar{u}_i$ denotes the mean velocity component in the i-th direction, and x_i represents the corresponding spatial coordinate. The overbar indicates a time-averaged (Reynolds-averaged) quantity, and the repeated index i implies summation over all spatial directions, in accordance with the Einstein summation convention. This equation enforces the conservation of mass for incompressible turbulent flows and serves as a fundamental constraint in the formulation of Reynolds-averaged Navier–Stokes (RANS) models [43].

For turbulent incompressible flow under steady-state conditions, the Reynolds-averaged Navier–Stokes (RANS) equations represent the momentum conservation laws in terms of time-averaged quantities. Using indicial notation and applying the Reynolds decomposition, the RANS equations are expressed as:

$$\bar{u}_j \frac{\partial \bar{u}_i}{\partial x_j} = -\frac{1}{\rho}\frac{\partial \bar{p}}{\partial x_i} + \nu \frac{\partial^2 \bar{u}_i}{\partial x_j \partial x_j} - \frac{\partial \overline{u_i' u_j'}}{\partial x_j} + g_i \tag{2}$$

where $\bar{u}_i$ and $\bar{u}_j$ denote the mean velocity components in the i- and j- direction, respectively, ρ is the fluid density, ν is the kinematic viscosity, $\bar{p}$ is the mean pressure. The term $ui'uj'$ represents the components of the Reynolds stress tensor, which arise from the nonlinear convective terms after Reynolds averaging. This additional stress term captures the influence of turbulence on the mean flow and introduces a closure problem due to the presence of unknown correlations between velocity fluctuations. Consequently, turbulence models—such as the Boussinesq hypothesis or two-equation models like the k-ε or k-ω models —are required to approximate the Reynolds stresses and achieve closure of the RANS equations.

Under steady-state conditions, the conservation of energy for turbulent incompressible flow is governed by the Reynolds-averaged energy equation. Expressed in indicial notation, the equation is given by:

$$\bar{u}_j \frac{\partial \bar{T}}{\partial x_j} = \alpha \frac{\partial^2 \bar{T}}{\partial x_j \partial x_j} - \frac{\partial \overline{u_j' T'}}{\partial x_j} \tag{3}$$

where $\bar{T}$ denotes the mean temperature, $\bar{u}_j$ is the time-averaged velocity component in the j- direction, and $\alpha = k/(\rho c_p)$ represents the thermal diffusivity, with k being the thermal conductivity, ρ the fluid density, and c_p the specific heat at constant pressure. The term $\overline{u_j' T'}$ corresponds to the turbulent heat flux, which arises from the correlation between temperature and velocity fluctuations. This additional term captures the effect of turbulent mixing on heat transport and introduces a closure problem analogous to the Reynolds stress in the momentum equation. To model the turbulent heat flux, it is common to invoke the gradient diffusion hypothesis, which approximates $\overline{u_j' T'} = -(\nu_t / Pr_t)(\frac{\partial \bar{T}}{\partial x_j})$, where ν_t is the turbulent eddy viscosity and Pr_t is the turbulent Prandtl number. This modeling approach enables closure of the energy equation within the framework of Reynolds-averaged turbulence models.

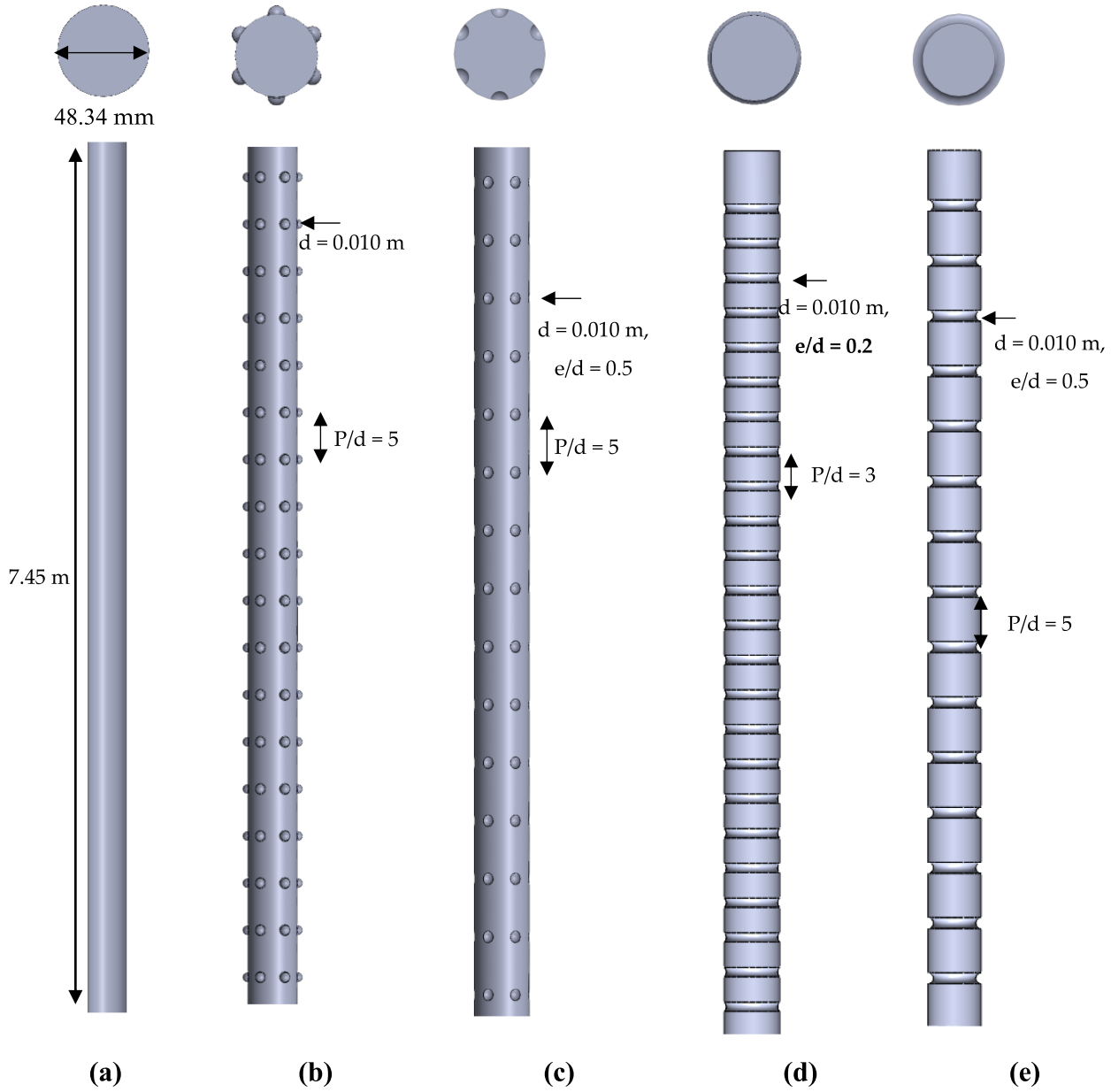

Fig. 1. The configurations of the 7.45 m heat pipe considered in this work. (a) smooth pipe, (b) pipe with spherical convex dimples, (c) pipe with concave spherical dimples, (d) pipe with circumferential grooves of normalized depth to diameter ratio (e/d) of 0.20, and (e) pipe with grooves with $e/d = 0.50$.

The presented CFD methodology was implemented using the Reynolds Stress Model (RSM) model with the enhanced wall function, due to its capability for turbulent internal pipe flows and its affordable computational cost. One limitation of this approach is that the RANS-based turbulent model cannot fully resolve the small-scale turbulence eddies near the wall at high Reynolds numbers. One approach to resolving small-scale turbulence structures is to use the Large Eddy Simulation (LES) turbulent model, which incurs a high computational cost [44]. It is worth noting that the presented work aims to study the overall thermal-hydraulic performance of the investigated geometries rather than the instantaneous detailed turbulent characteristics.

After solving Eqs. (1) to (3) numerically during the CFD simulation, the average flow velocity, the static pressure, and the temperature were extracted and used to calculate the average convective heat transfer coefficient, the Nusselt number, pressure drop, and

the friction factor for each case. The Nusselt number (Nu) is calculated using the following Equation:

$$Nu = \frac{h_{ave} D_h}{k} \tag{4}$$

where h_{ave}, D_h and k are the average convective heat transfer coefficient, hydraulic diameter, and the thermal conductivity of the fluid, respectively. For a known heat flux, the average convective heat transfer coefficient can be obtained from the following Equation:

$$h_{ave} = \frac{q''}{T_w - T_b} \tag{5}$$

where q'', T_w, and T_b are the heat flux at the wall, the wall's temperature, and the fluid bulk temperature at the cross section, respectively. In this study, a constant heat flux (8,800 W/m^2) was used as the boundary condition at the wall, and it was not extracted from the CFD results. Whereas the wall temperature (T_w) was obtained from the CFD results as the area-weighted average at the heated wall. To obtain the fluid bulk temperature, the temperature at the inlet (T_{in}) and outlet (T_{out}) were determined as the mass-weighted average at the inlet and outlet of the computational domain, respectively. Then, the fluid bulk temperature (T_b) was calculated using Eq. (6). The average convective heat transfer coefficient was then calculated using Eq. (5).

$$T_b = \frac{T_{in} + T_{out}}{2} \tag{6}$$

Static pressure was extracted at the inlet and outlet of the heated pipe to determine the pressure drop and calculate the friction factor (fr) using Eq. (7):

$$fr = \frac{2\Delta p D}{\rho L u^2} \tag{7}$$

where Δp,ρ, L, and u are the pressure drop, fluid density, length of the pipe, and the bulk fluid velocity. The bulk flow velocity was extracted at a plane located at 6.325 m from the inlet. The thermal performance factor (TPF) was evaluated, which indicates the heat transfer enhancement performance compared to the smooth pipe. It is defined as the ratio of the Nusselt number of the modified pipe to the smooth pipe to the ratio of the friction factor of the modified pipe to the smooth pipe, as shown in Eq. (8) [45].

$$TPF = \frac{Nu_{with\ modification}/Nu_{smooth\ pipe}}{(fr_{with\ modification}/fr_{smooth\ pipe})^{\frac{1}{3}}} \tag{8}$$

In addition, the CFD results of the Nusselt number with different values of Reynolds number under the smooth pipe geometry were compared with the Gnielinski correlation using Eq. (9) [46].

$$Nu = \frac{\left(\frac{fr}{8}\right)(Re - 1000)\ Pr}{1 + 12.7\sqrt{fr/8}\ \left(Pr^{\frac{2}{3}} - 1\right)} \tag{9}$$

where fr is the friction factor, and Pr is the Prandtl number.

2.3. CFD simulation setup

The simulations were conducted using ANSYS Fluent 2023. All pipes were modeled as stainless steel, with water at atmospheric pressure as the working fluid. The flow is assumed to be steady, incompressible, and the thermal physical properties are constant. Default material properties provided in ANSYS [43] (Table 1) were applied to all geometries (Fig. 1). Each pipe included three boundary conditions: velocity inlet, pressure outlet, and heated wall (Fig. 2). The inlet velocity ranged from 0.62 to 1.18 m/s, which corresponds to Reynolds numbers from 30000 to 57000. The inlet temperature was 19.1 °C, and the thermal-physical properties of water and steel were assumed constant, as the water temperature rise along the heated pipe was moderate. Thus, the effect of temperature on the properties in the presented CFD simulations is negligible. The pressure outlet boundary condition with zero-gauge pressure was imposed at the outlet. The wall was treated as no-slip with a constant heat flux of 8,800 W/m^2. The Reynolds numbers and the constant wall heat flux were chosen based on the experimental data used for the CFD validation of the temperature distribution [35]. Turbulence intensity and viscosity ratio at both the inlet and the outlet were set to 5% and 10%, respectively.

Table 1. Properties of the working fluid and the solid material of the pipe geometry, adopted from ANSYS Fluent Theory Guide [43].

Property	Value
Water	
Density (kg/m^3)	998.2
Specific heat (J/kg.K)	4182
Thermal conductivity (W/m.K)	0.6
Viscosity (kg/m.s)	0.001003
Inlet velocity (m/s)	0.62–1.18 m/s
Inlet temperature	19.1 °C
Steel pipe	
Density (kg/m^3)	8030
Specific heat (J/kg.K)	502.48
Thermal conductivity (W/m.K)	16.27

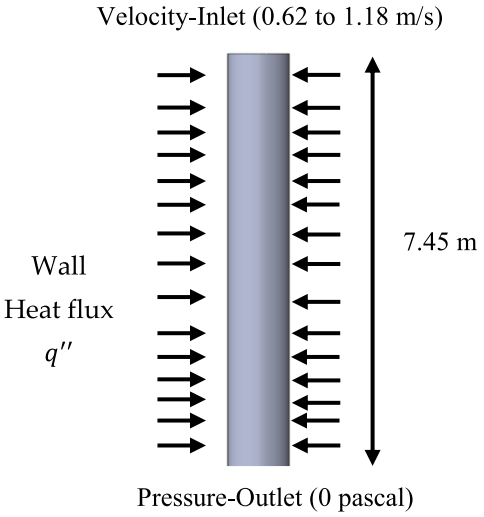

Fig. 2. Illustration of the boundary conditions.

The Reynolds Stress Model (RSM) is used to simulate turbulent internal pipe flow and has been shown to provide reliable predictions of turbulent flow and flow separation [47]. The enhanced wall function was used to accurately resolve the viscous sublayer and to ensure the y^+ value is below ~5 [43]. In the presented heat transfer simulations, the obtained $y^+ \approx 1$. Pressure–velocity coupling used the SIMPLEC algorithm to improve the convergence of the turbulent flow [43]. The spatial discretization of pressure employed the PRESTO scheme to enhance the accuracy of the pressure gradient prediction resulting from the surface pipe modifications. All transport equations were discretized using second-order upwind schemes. Convergence criteria were set to 10^{-4} for continuity and 10^{-9} for energy. The presented CFD simulation was performed in the vertical orientation, and gravity was accounted for.

2.4. Grid independence study and CFD validation strategies

Two grid independence studies were conducted in this work: one for the smooth pipe and another for the dimpled pipe. A poly-hexacore mesh was employed for all simulations.

2.4.1. Smooth pipe

To assess mesh sensitivity, five progressively refined meshes (20% refinement ratio) were generated for the smooth pipe case (Fig. 1(a)). The first mesh employed a face size of 1.15×10^{-3} m at the inlet and outlet, with a first-layer thickness of 2.30×10^{-5} m. The second mesh was refined by 20%, resulting in a face size of 9.60×10^{-4} m and a first-layer thickness of 1.92×10^{-5} m. The same refinement procedure was applied to obtain the remaining three meshes. All meshes maintained a minimum orthogonal quality of 0.52. The mesh sensitivity study was conducted at a Reynolds number of 57,000. Numerical results were validated against the experimental data of Jackson et al. [35] by comparing the radial temperature distribution at a pipe cross-section located 6.325 m downstream of the inlet. The temperature profiles obtained from the five meshes are presented in Fig. 3.

As shown in Fig. 3, the radial temperature distribution remained essentially unchanged as the mesh density increased from 736k to 2.6M cells. To further assess grid sensitivity, absolute temperature differences were evaluated at a radius of 20 mm, located 6.325 m downstream of the inlet (Table 2). The temperature difference decreased with mesh refinement: the largest deviation was 0.017 °C (mesh #1 vs. mesh #2), while the smallest was 0.003 °C (mesh #3 vs. mesh #4). Comparisons with the experimental data of Jackson et al. [35] also showed improved agreement with increasing cell count. The average absolute deviation from experimental data was approximately 0.49 °C, and the difference between mesh #4 and mesh #5 relative to the experimental data was only 1.66%. Therefore, mesh #4 was selected for subsequent simulations of both smooth and modified pipe configurations.

2.4.2. Dimpled pipe

For validation of the CFD model for dimpled pipes, an experimental case from Al-Haidari et al. [41] was adopted. The test section consists of a 23 mm diameter copper pipe with three spherical dimples (Fig. 4). Water was used as the working fluid at $Re = 15,000$ under a constant heat flux of 25,500 W/m^2. A mesh sensitivity study was first conducted using five meshes (1.651–5.341 million elements). The Nusselt number and friction factor were computed for each mesh and compared with experimental data (Fig. 5). The maximum percentage changes in the Nusselt number and the friction factor were observed 1.69% and 4.08%, respectively, when the mesh was refined from mesh #2 to mesh #3. Compared with experimental data, mesh #2 yielded deviations of 18.72% for Nu and about 4.08% for the friction factor. Accordingly, mesh #2 was selected for further validation at different Reynolds numbers. Fig. 6 presents the cross-sectional view of the validation mesh, while Table 3 summarizes the mesh statistics and deviations. Fig. 7 shows representative front and cross-sectional views of the meshes used in the present study.

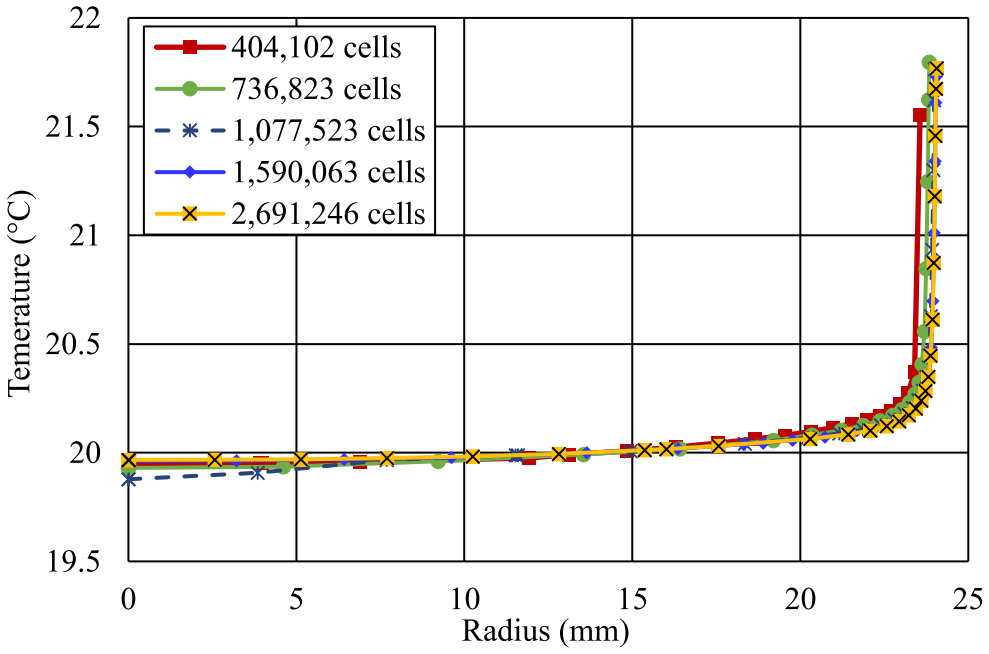

Fig. 3. Results of mesh sensitivity study across the radial direction of smooth pipe (Fig. 1(a)) at a distance from the inlet flow section of 6.325 m.

Table 2. Grid sensitivity study of smooth pipe results and comparison with Jackson et al. [35] experimental data.

Mesh No.	No. of cells	T_b (°C)	$\lvert\Delta T_b\rvert_{mesh}$ (°C)	$\lvert\Delta T_b\rvert_{CFD\text{-}Exp}$ (°C)
1	404,102	20.098	0.017	0.511
2	736,823	20.081		0.494
3	1,077,523	20.069	0.012	0.482
4	1,590,063	20.072	0.003	0.485
5	2,691,246	20.064	0.008	0.477
Exp. Data from Jackson et al. [35]	-	19.587	-	-

Note: $\lvert\Delta\rvert_{mesh}$ refers to the absolute difference between the sequential meshes.
$\lvert\Delta\rvert_{CFD\text{-}Exp}$ refers to the absolute difference between the CFD prediction and the experimental data.



Fig. 4. The geometry of the adopted dimpled pipe from Al-Haidari et al. [41].

Table 3. Grid sensitivity study for the dimpled pipe and comparison with experimental data from Al-Haidari et al. [41].

Mesh No.	No. of cells	*Nu*	$\lvert\Delta Nu\rvert_{mesh}$ (%)	$\lvert\Delta Nu\rvert_{CFD\text{-}Exp}$ (%)	*fr*	$\lvert\Delta fr\rvert_{mesh}$ (%)	$\lvert\Delta fr\rvert_{CFD\text{-}Exp}$ (%)
1	1,651,431	135.94	1.29	20.27	0.0546	2.86	6.53
2	2,546,853	134.19	1.69	18.72	0.0531	4.08	9.20
3	3,299,004	136.45	1.24	20.72	0.0552	3.89	5.50
4	4,512,644	134.75	0.58	19.22	0.0531	0.02	9.17
5	5,341,304	135.53		19.91	0.0531		9.16
Exp. Data from Al-Haidari et al. [41]	-	113.03			0.0584	-	-

Note: $\lvert\Delta\rvert_{mesh}$ refers to the absolute difference between the sequential meshes.
$\lvert\Delta\rvert_{CFD\text{-}Exp}$ refers to the absolute difference between the CFD prediction and the experimental data.

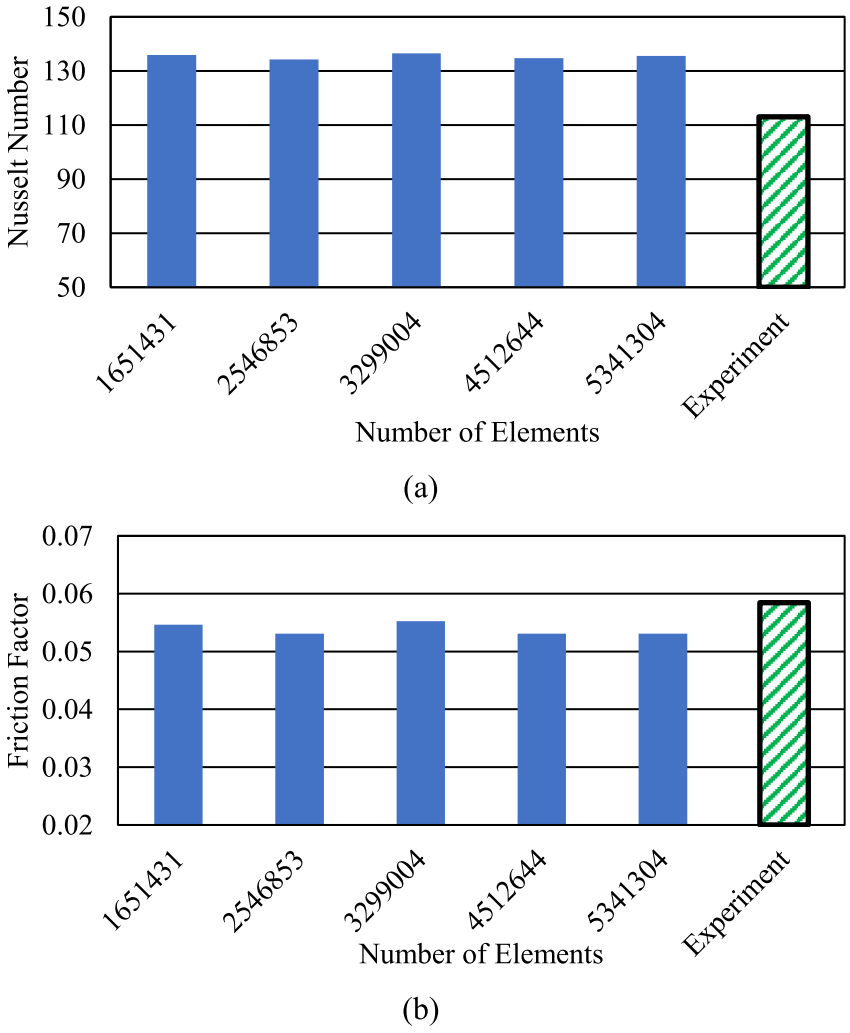

Fig. 5. Mesh sensitivity study of the dimpled pipe: (a) Nusselt number, and (b) friction factor.

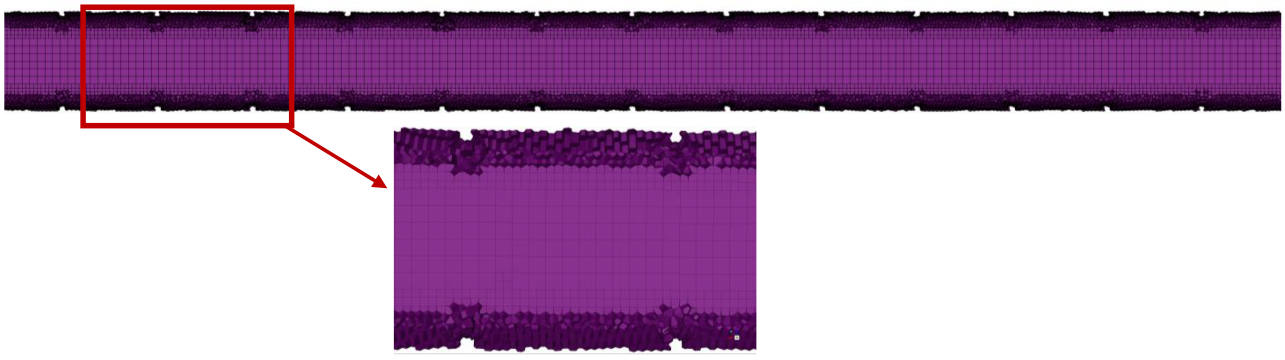

Fig. 6. Views of mesh #2 of the dimpled pipe for CFD validation.

3. Results and discussion

3.1. CFD validation of the smooth pipe

The CFD model was validated against the experimental temperature distribution reported by Jackson et al. [35] for a smooth pipe at a location 6.325 m downstream of the inlet. As shown in Fig. 8, the CFD predictions closely follow the experimental trend, with a slight temperature increase from the centerline up to about 20 mm, followed by a sharper rise near the wall. The maximum absolute temperature

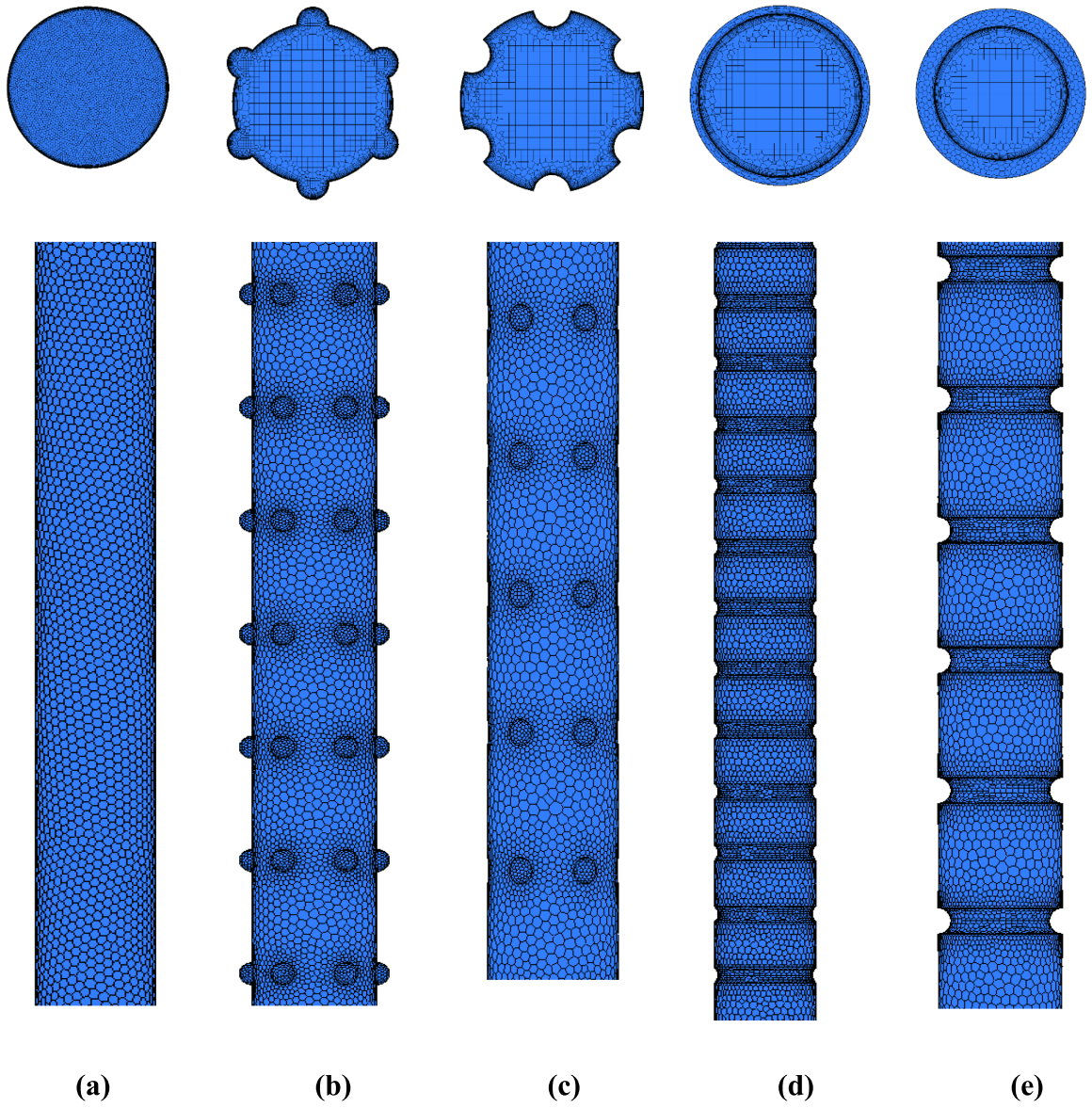

Fig. 7. Mesh configuration of (a) smooth pipe, (b) pipe with spherical convex dimples, (c) pipe with concave spherical dimples, and (d) pipe with circumferential grooves of normalized depth to diameter ratio (e/d) of 0.20, and (e) pipe with grooves with e/d=0.50.

difference between CFD and experimental data was less than 0.6 °C. For example, at the pipe centerline, the CFD predicted 19.96 °C compared to 19.39 °C experimentally. Similar small deviations were observed at $r = 3.22$, 9.62, 12.82, and 20.73 mm, confirming good agreement and supporting the validity of the numerical model.

Both CFD and experimental results show a gradual temperature increase with radius, followed by a sharp rise beyond $r \approx 22$ mm, reaching 21.73 °C (CFD) and 21.97 °C (experiment). This behavior is expected due to the constant heat flux applied at the pipe wall. The steep temperature gradient near the wall is attributed to the development of the thermal boundary layer, where heat is transferred from the heated surface to the cooler fluid core. Turbulence also plays an important role in this region. As reported by He [48], turbulence intensity is significantly higher near the wall—particularly in the radial and tangential components—enhancing heat transfer. Moving away from the wall, turbulent fluctuations, shear stress, and turbulent kinetic energy decrease, reducing convective mixing and leading to a more uniform temperature near the pipe centerline. The close agreement between CFD and experimental profiles confirms the reliability of the present numerical model in accurately capturing the thermal behavior of turbulent flow in a heated pipe.

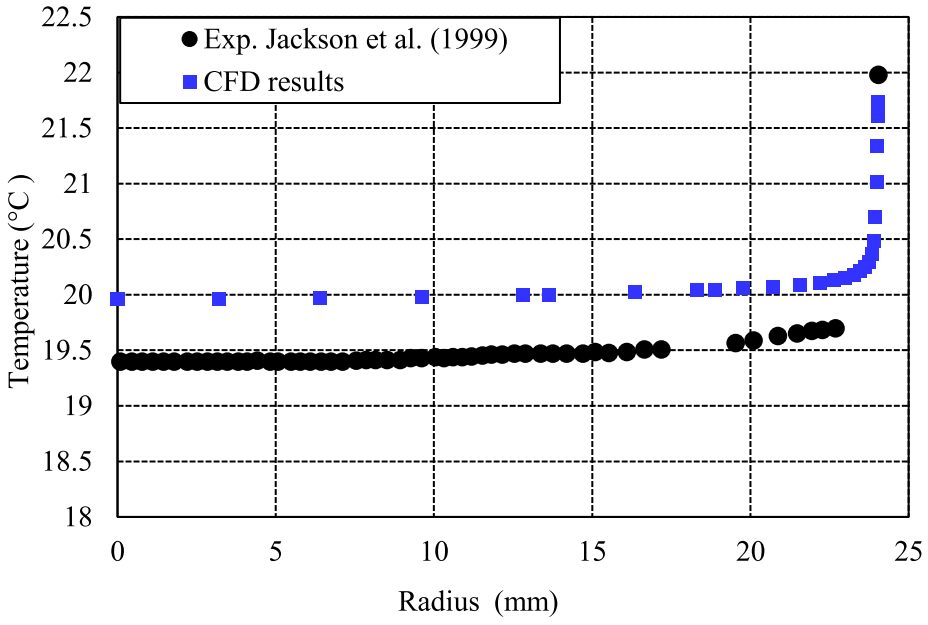

Fig. 8. The temperature distribution across the radial direction of the pipe at 6.325 m from the pipe's inlet.

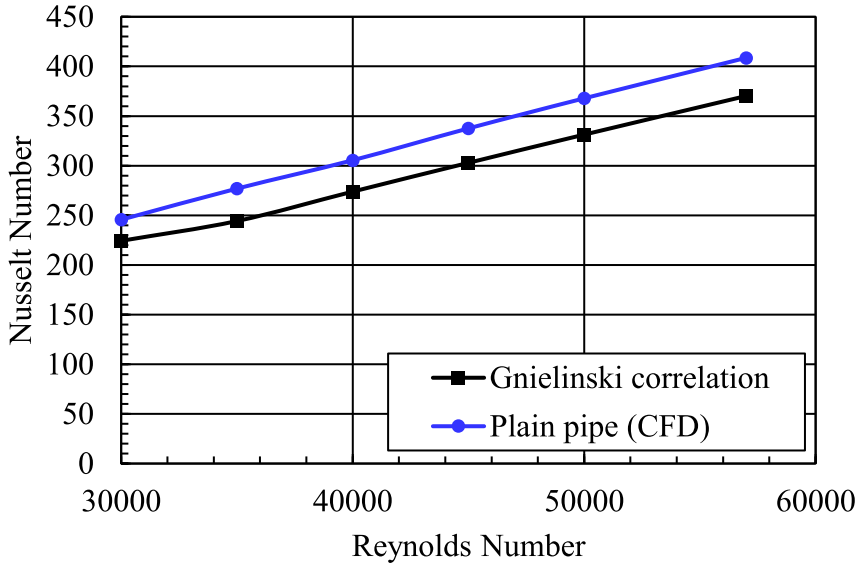

Fig. 9. The CFD results of the Nusselt number vs. Gnielinski correlation of the smooth pipe.

The Nusselt number predicted for the smooth pipe at different Reynolds numbers was also compared with the Gnielinski correlation [46] (Fig. 9). The CFD results show good agreement with the correlation and follow the same trend, where the Nusselt number increases with increasing Reynolds number, reflecting enhanced convective heat transfer. The maximum deviation between the CFD predictions and the Gnielinski correlation was approximately 13% at $Re = 35{,}000$. This difference may be attributed to uncertainties in the CFD setup—such as the turbulence model, wall treatment, and boundary conditions—as well as the assumptions and experimental basis underlying the Gnielinski correlation.

3.2. CFD validation of the dimpled pipe

The CFD model was further validated against the experimental data of Al-Haidari et al. [41] for Reynolds numbers between 4000 and 15,000 (Fig. 10 a, b). For the Nusselt number, the CFD underpredicted the results at low Reynolds numbers (38.8% at $Re = 4000$ and 19.6% at $Re = 6000$). At higher Reynolds numbers (10,000–15,000), the model

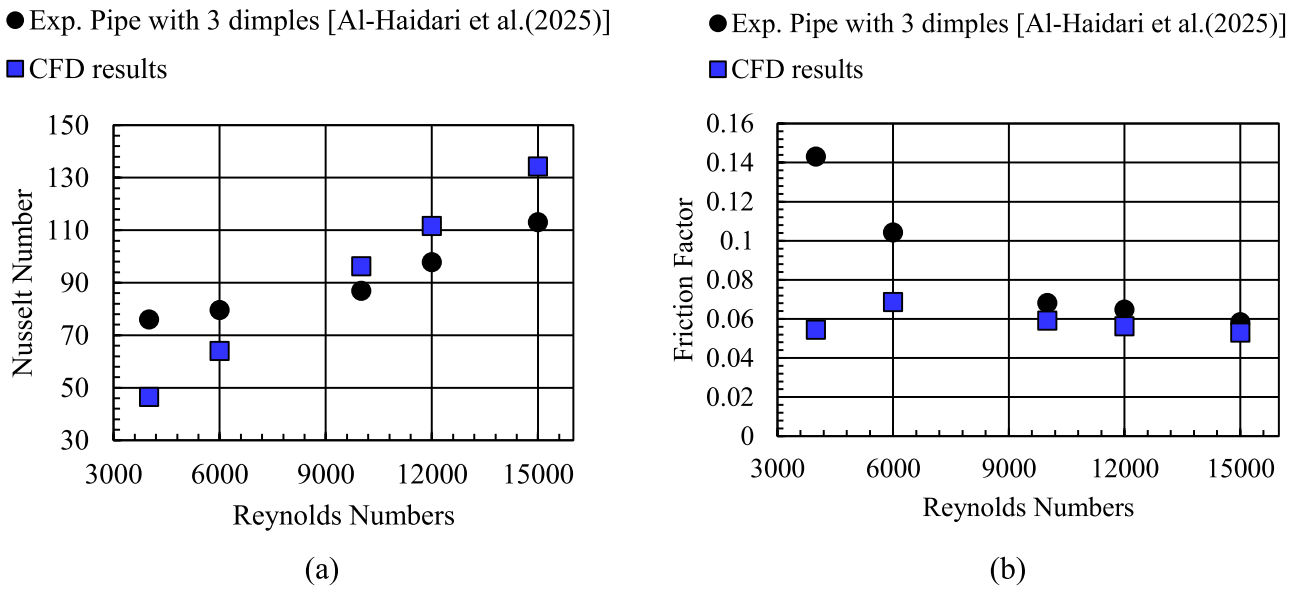

Fig. 10. The CFD results vs. experimental data of the dimpled pipe: (a) Nusselt number, and (b) friction factor.

slightly overpredicted Nu, with deviations of 10.8%, 14.1%, and 18.7%, respectively. Similarly, for the friction factor, the CFD significantly underpredicted the values at $Re = 4000$ and 6000 (62% and 34%, respectively), while showing improved agreement at higher Reynolds numbers, with a maximum deviation of about 13% at $Re = 10{,}000$. The larger discrepancies at low Reynolds numbers may be attributed to transitional flow effects, where the flow is not fully turbulent and the RSM turbulence model may not accurately capture the physics. A detailed assessment of different turbulence models at $Re \leq 6000$ would be required for improved prediction. Overall, the CFD and experimental data exhibit consistent trends: the Nusselt number increases with Reynolds number, while the friction factor decreases.

3.3. Velocity fields

The velocity fields, pressure gradients, and temperature distributions were analyzed, as they are the key factors governing the mechanisms of heat transfer enhancement and the friction factor in the modified pipe configurations. Velocity vectors and contours for the five pipe configurations at $Re = 57{,}000$ are shown in Fig. 11(a–e), evaluated at 6.325 m from the inlet. For the smooth pipe (case a), the velocity profile is uniform and fully developed, with no surface features disturbing the boundary layer. The maximum velocity is 1.4 m/s at the pipe core, decreasing gradually toward the wall. In contrast, cases (b)–(e) exhibit higher centerline velocities due to flow disturbance caused by dimples and grooves. The maximum velocity increases progressively, reaching 2.81 m/s in case (e), where grooves reduce the effective flow area and create partial blockage. The absolute differences in average velocity (relative to case a) are 0.12, 0.14, 0.22, and 0.67 m/s for cases (b), (c), (d), and (e), respectively. These surface modifications generate recirculation and enhanced mixing near the wall, shifting momentum toward the core region and promoting improved convective heat transfer.

3.4. Pressure gradients

The effect of Reynolds number on pressure drop for cases (a)–(e) is shown in Fig. 12. In all configurations, the pressure drop increases with Reynolds number due to higher flow velocity. Compared to the smooth pipe (case a), the dimpled and grooved pipes exhibit significantly higher-pressure drops, caused by flow separation and recirculation induced by surface modifications. This effect becomes more pronounced at higher Reynolds numbers. The static pressure distribution along the pipe length and at 7 m from the inlet ($Re = 57{,}000$) is presented in Figs. 13 and 14(a–e). The modified pipes (b–e) show consistently higher-pressure levels than the smooth pipe. The total pressure drops for cases (a), (b), (c), (d), and (e) are 2434, 3180, 6174, 11805, and 33406 Pa, respectively. This corresponds to increases of 31%, 154%, 385%, and 1272% for cases (b), (c), (d), and (e), relative to the smooth pipe. Case (e) exhibits the highest pressure drop due to its deep grooves, which significantly increase the friction factor. Although this configuration enhances mixing, the associated

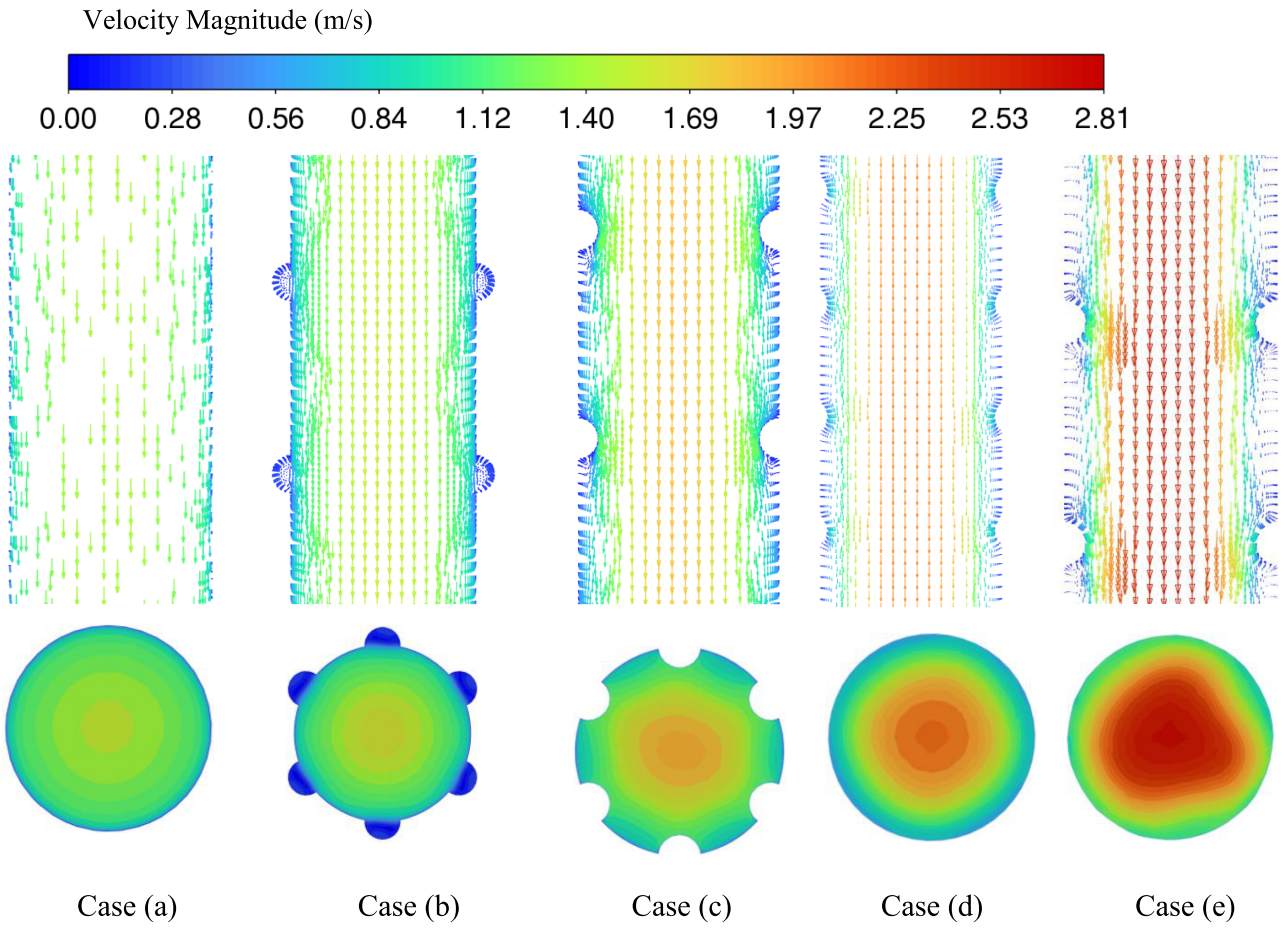

Fig. 11. The velocity vectors and distributions: (a) smooth pipe, (b) pipe with spherical convex dimples, (c) pipe with concave spherical dimples, and (d) pipe with circumferential grooves of normalized depth to diameter ratio (e/d) of 0.20, and (e) pipe with grooves with $e/d = 0.50$ with an inlet velocity of 1.18 m/s.

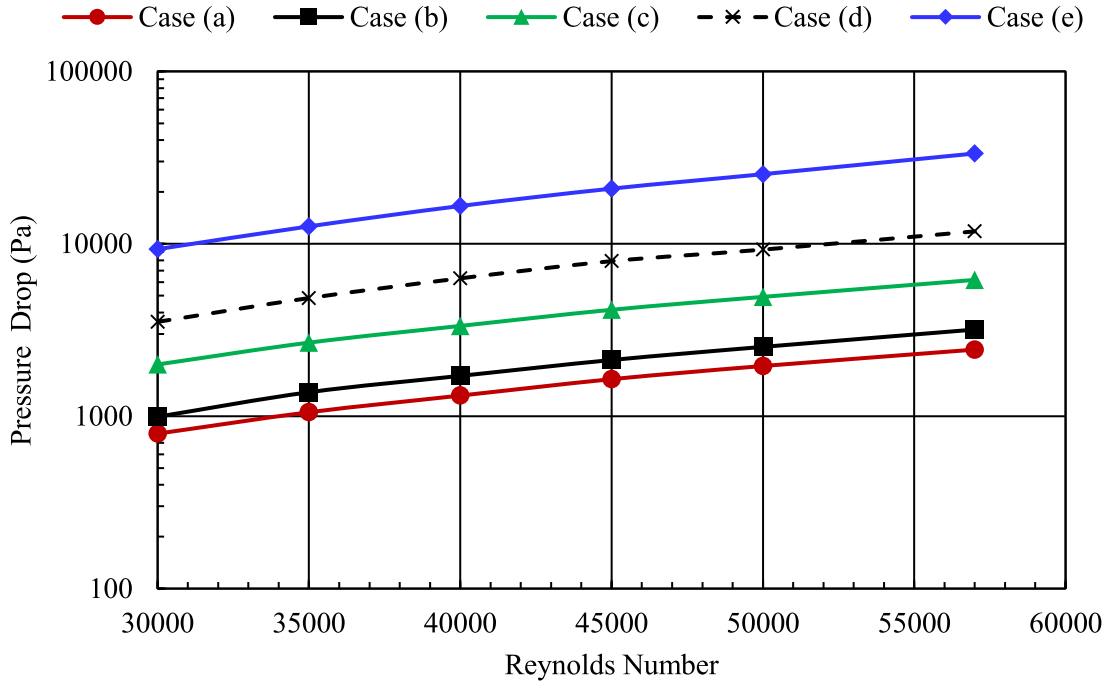

Fig. 12. The effect of the Reynolds number on the pressure drop for the investigated pipe geometries.

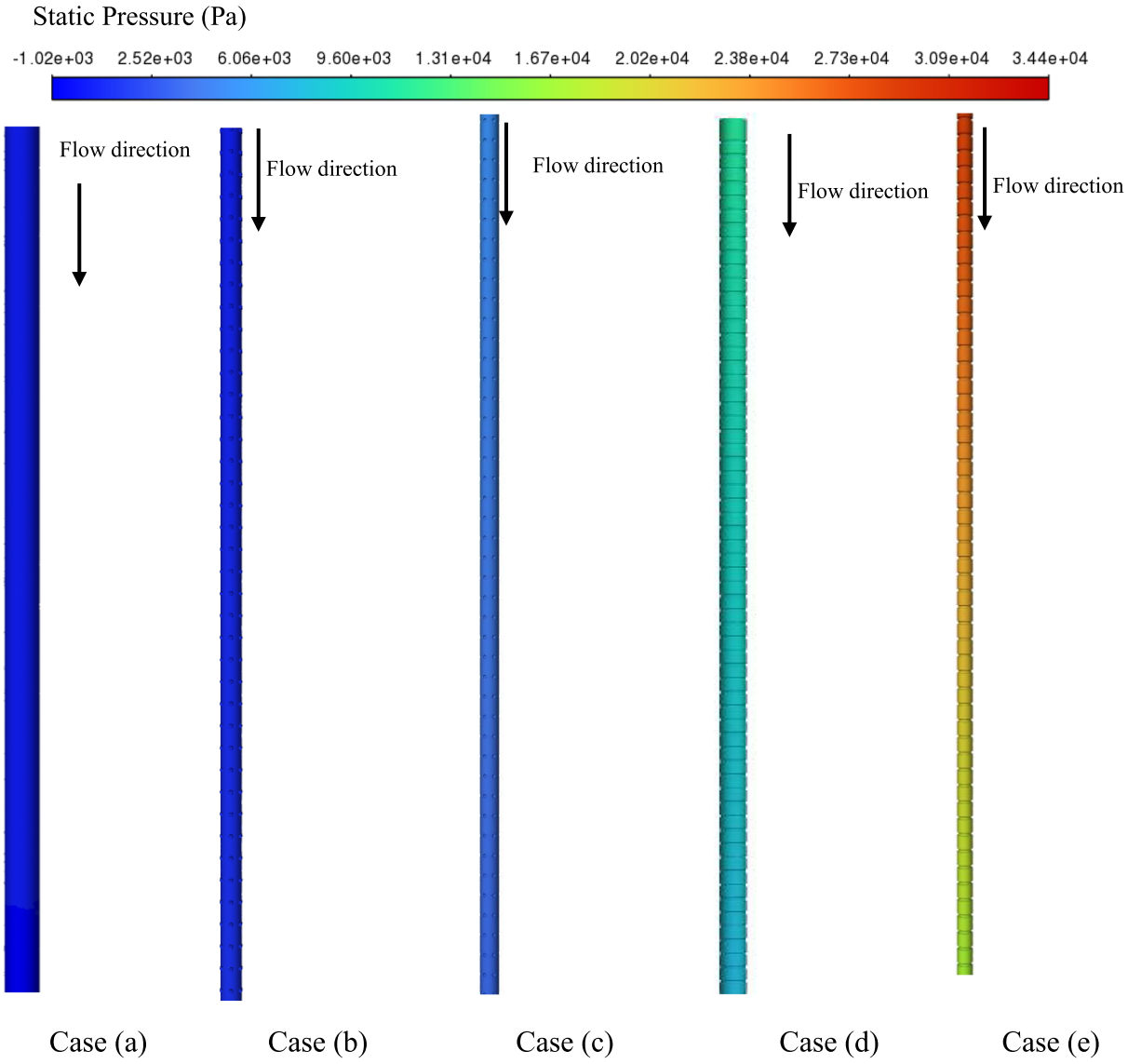

Fig. 13. The static pressure distribution: (a) smooth pipe, (b) pipe with spherical convex dimples, (c) pipe with concave spherical dimples, and (d) pipe with circumferential grooves of normalized depth to diameter ratio (e/d) of 0.20, and (e) pipe with grooves with e/d=0.50 with an inlet velocity of 1.18 m/s.

pressure penalty suggests higher pumping power requirements, making it less favorable from an overall performance standpoint.

3.5. Temperature distributions

The temperature distributions for all five geometries were analyzed at $Re = 57{,}000$ (Fig. 15(a–e)). In all cases, the fluid temperature increased along the flow direction due to the applied heat flux. The smooth pipe (a) and the pipe with external dimples (b) exhibited the highest average wall temperatures: 21.4 °C and 21.3 °C, respectively. Lower average wall temperatures were observed for cases (c), (d), and (e): 20.9 °C, 20.6 °C, and 20.4 °C, respectively. The reduced wall temperatures in the protruded and grooved pipes are attributed to enhanced near-wall turbulence and mixing, which disrupts the thermal boundary layer. From case (c) to (e), the decreasing wall temperature indicates improved convective heat transfer, reflected in higher heat transfer coefficients and Nusselt numbers. In contrast, the higher wall temperatures in cases (a) and (b) correspond to weaker mixing, lower heat transfer coefficients, and reduced thermal performance.

3.6. Turbulent kinetic energy (TKE)

The turbulent kinetic energy was examined in the downstream section (6.325 m from the inlet) for

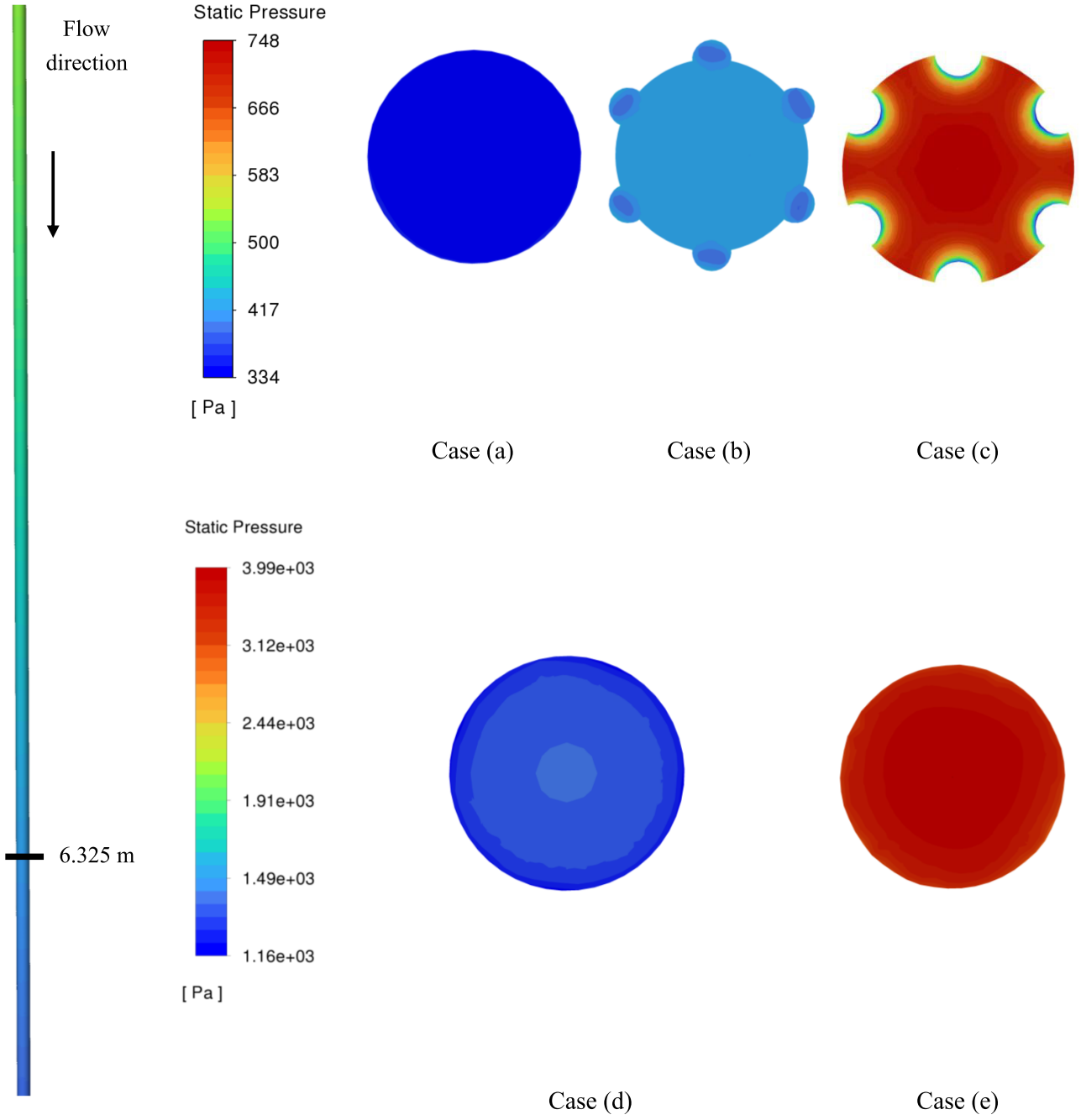

Fig. 14. The static pressure distribution located at 6.325 m from the inlet: (a) smooth pipe, (b) pipe with spherical convex dimples, (c) pipe with concave spherical dimples, and (d) pipe with circumferential grooves of normalized depth to diameter ratio (e/d) of 0.20, and (e) pipe with grooves with $e/d = 0.50$ with an inlet velocity of 1.18 m/s.

all five pipe geometries at the Reynolds number of 57,000, as shown in Fig. 16. The CFD results showed a substantial increase in the turbulent kinetic energy near the wall for the surface-modified pipes compared to the smooth pipe. The average turbulent kinetic energy was increased by 32% for case (b) due to the presence of convex dimples, which disturb the near-wall boundary layer and enhance mixing. For the concave dimples (case c), the average turbulent kinetic energy increased by 99%, leading to stronger near-wall interactions and improved heat transfer compared to the smooth pipe. In the grooved pipes (cases d and e), the average turbulent kinetic energy is further intensified, which increased by 278% and 788%, respectively. This increase in turbulent kinetic energy in the grooved pipes explains the higher

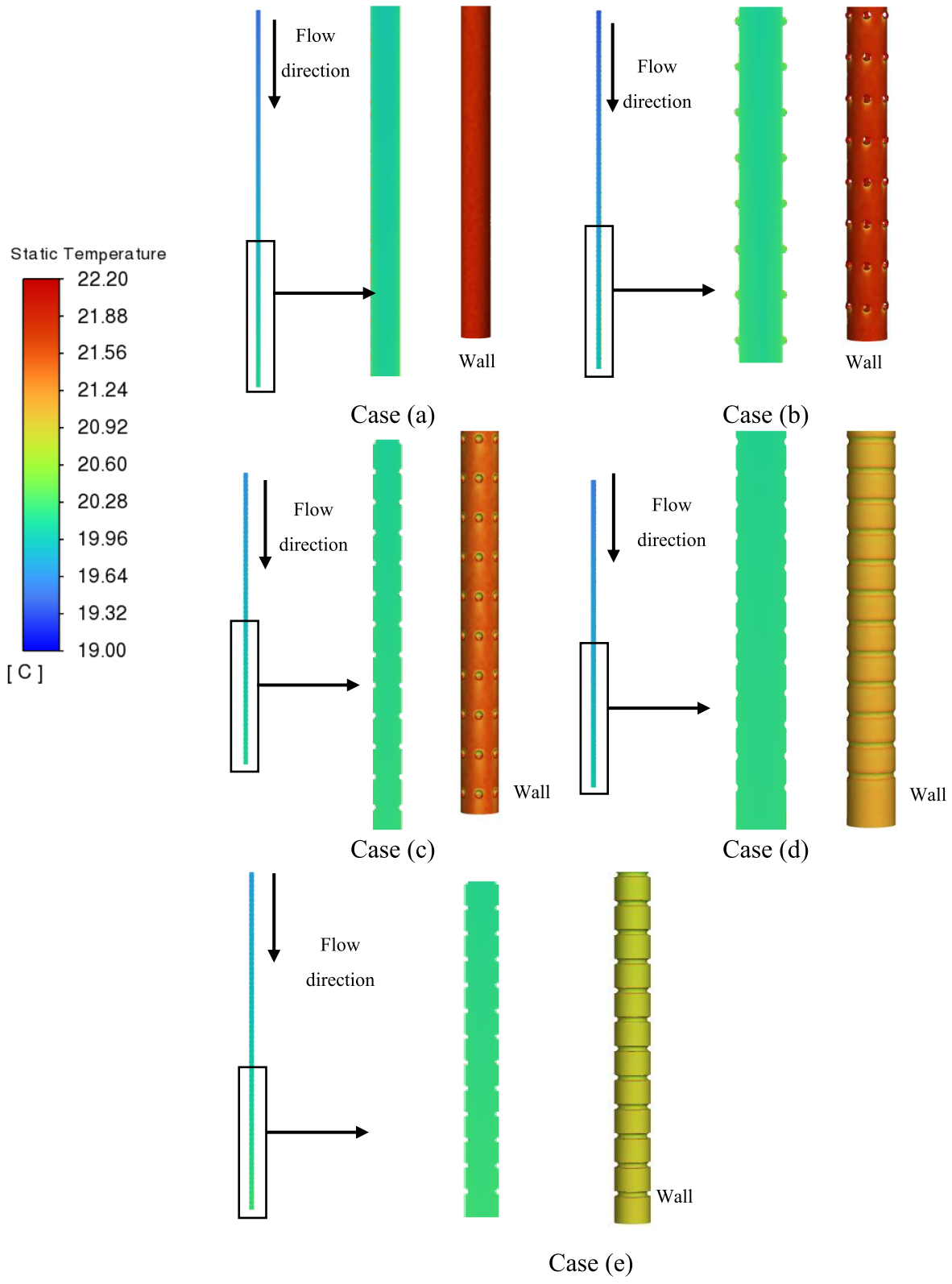

Fig. 15. The downstream temperature distribution at the midplane of the pipe and the walls: (a) smooth pipe, (b) pipe with spherical convex dimples, (c) pipe with concave spherical dimples, and (d) pipe with circumferential grooves of normalized depth to diameter ratio (e/d) of 0.20, and (e) pipe with grooves with e/d=0.50 with an inlet velocity of 1.18 m/s.

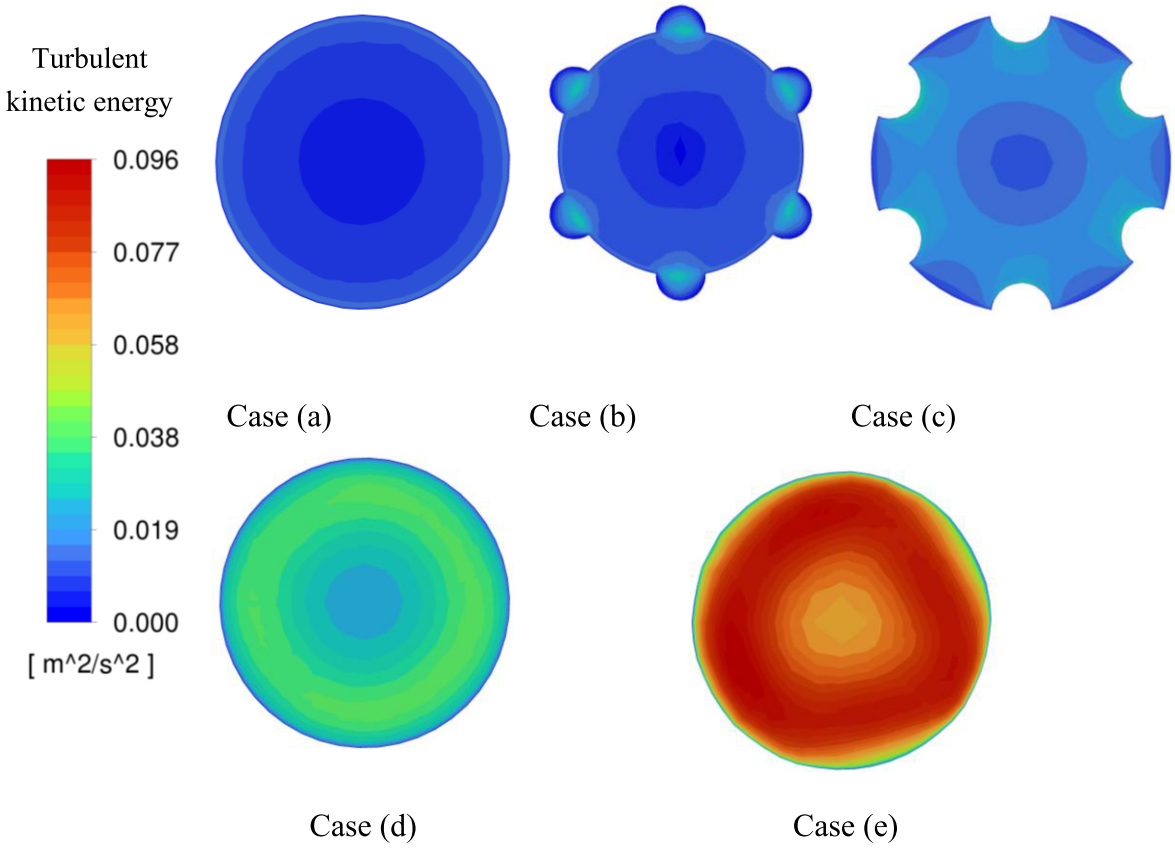

Fig. 16. The across view of the turbulent kinetic energy at around 6.325 m from the inlet: (a) smooth pipe, (b) pipe with spherical convex dimples, (c) pipe with concave spherical dimples, and (d) pipe with circumferential grooves of normalized depth to diameter ratio (e/d) of 0.20, and (e) pipe with grooves with e/d=0.50 with an inlet velocity of 1.18 m/s.

heat transfer enhancement observed in the present study, as shown in the following subsection. Indeed, the increase in the turbulent kinetic energy indicates greater flow separation and mixing due to the wall surface modification.

3.7. The effect of pipe geometry on Nu, fr, and TPF

Fig. 17 illustrates the effect of Reynolds number (30,000–57,000) on the Nusselt number for all investigated geometries. In every case, Nu increases with Reynolds number due to enhanced turbulence and thinner thermal boundary layers at higher flow rates. The smooth pipe (case a) consistently shows the lowest Nu values and serves as the baseline. The convex and concave dimpled pipes (cases b and c) improve heat transfer, with Nu approximately 1.2 and 1.4 times higher than the smooth pipe, respectively. The superior performance of concave dimples indicates more effective boundary-layer disruption and stronger turbulence generation within the core flow region. The grooved pipes (cases d and e) exhibit the highest enhancement. Case (d) ($e/d = 0.2$) achieves about 1.9 times the Nu of the smooth pipe, while case (e) ($e/d = 0.5$) provides the greatest improvement—approximately 2.4 times higher across the Reynolds number range. The deeper grooves intensify recirculation and mixing, resulting in stronger heat transfer enhancement. Notably, the relative performance of all geometries remains nearly constant with increasing Reynolds number, indicating that geometry-induced flow disturbances dominate the enhancement mechanism. Overall, internal grooves—particularly with larger depth—offer the most effective and consistent heat transfer improvement among the configurations studied.

Fig. 18 presents the variation of the friction factor (fr) with Reynolds number for all five geometries. For cases (a)–(d), the friction factor decreases gradually with increasing Reynolds number, consistent with turbulent pipe-flow behavior where viscous effects become less dominant at higher velocities. Compared to the smooth pipe (case a), the average friction factors increase by approximately 1.6 and 2.0 times for the convex and concave dimpled pipes (cases b and c), respectively, indicating moderate

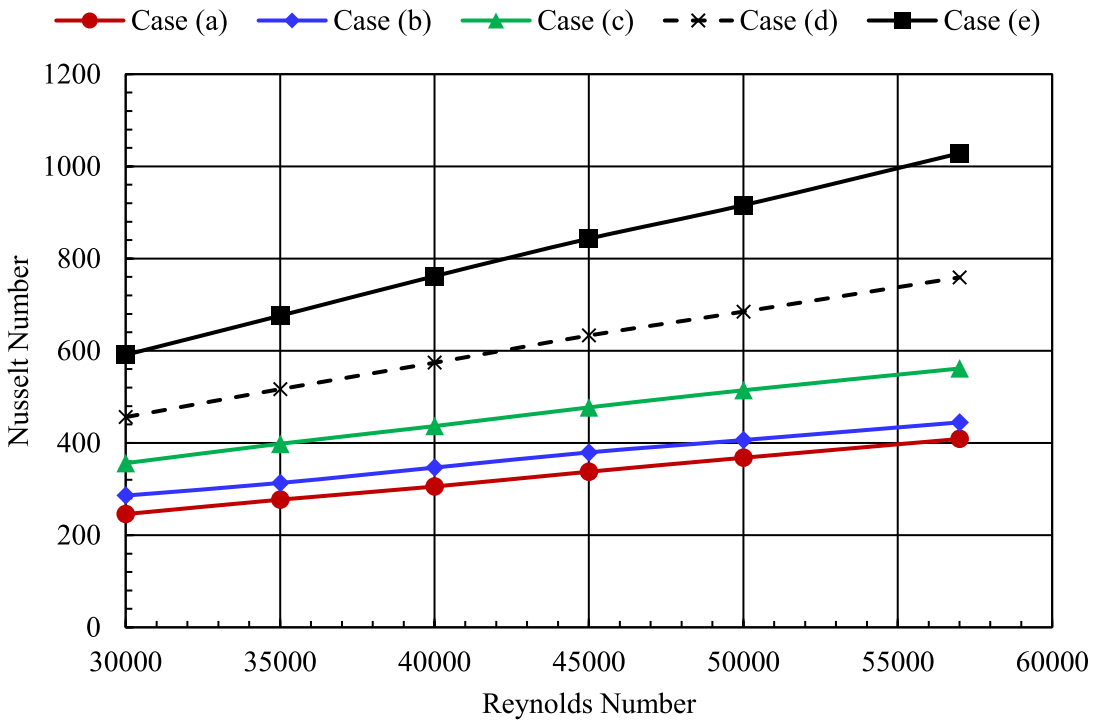

Fig. 17. The effect of the Reynolds number on the Nusselt number for the investigated pipe geometries.

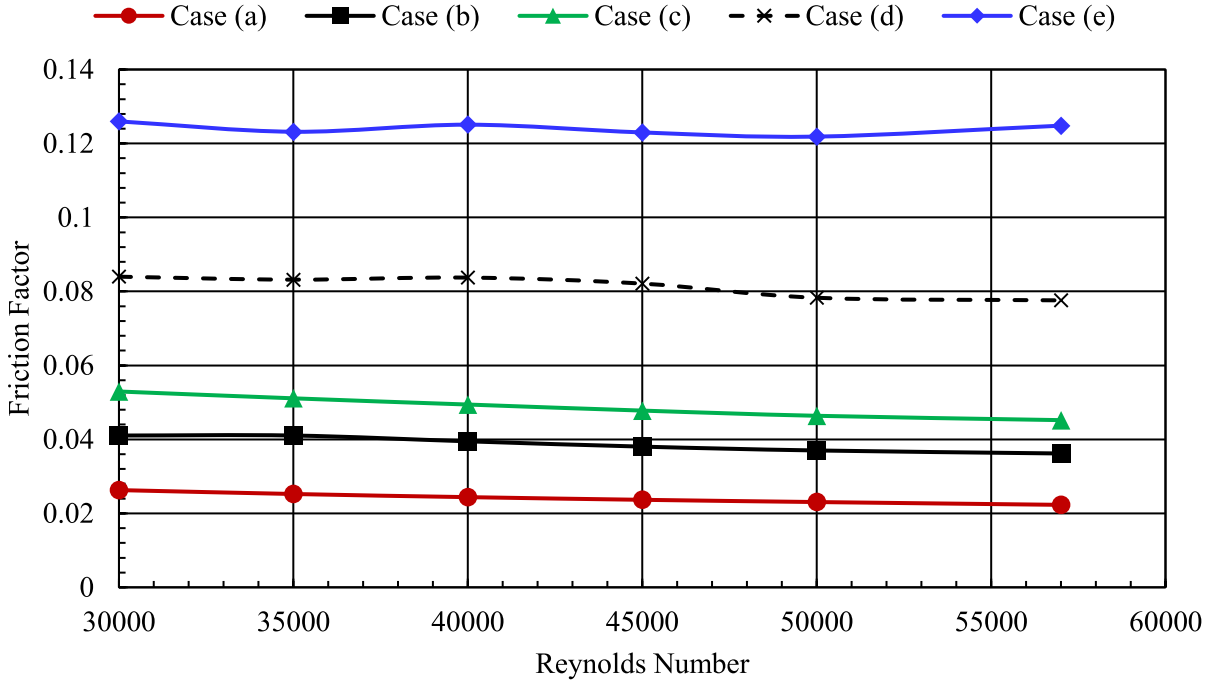

Fig. 18. The effect of the Reynolds number on the friction factor for the investigated pipe geometries.

additional flow resistance. Case (d), with shallow grooves ($e/d = 0.2$), exhibits a larger increase—about 2.5 times that of the smooth pipe—due to enhanced recirculation and turbulence. In contrast, case (e) ($e/d = 0.5$) shows an almost constant friction factor across the investigated Reynolds number range and the highest overall resistance, with an average value approximately 3.4 times that of the smooth pipe. The deeper grooves generate strong flow separation, vortex formation, and reattachment,

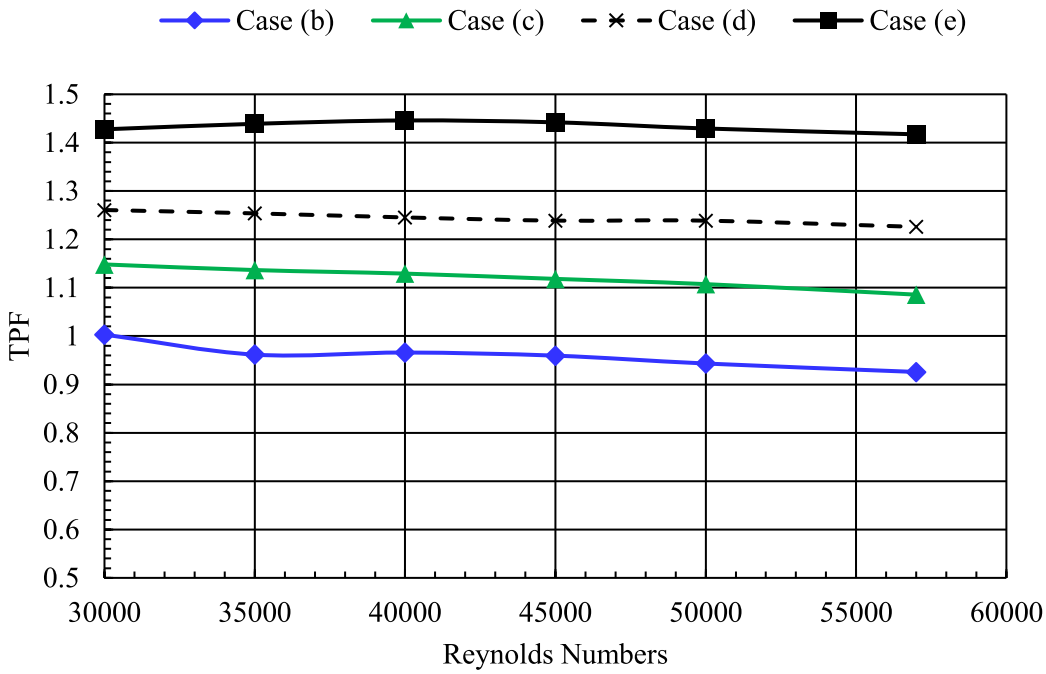

Fig. 19. The effect of the Reynolds number on the thermal performance factor (TPF) for the pipe geometries investigated.

significantly increasing pressure drop and wall shear stress. Overall, the results highlight a clear trade-off between heat transfer enhancement and hydraulic performance. While case (e) achieves the highest Nusselt number, it incurs a substantial friction penalty. Cases (b)–(d), however, provide more balanced performance by offering meaningful heat transfer enhancement with comparatively lower pressure losses.

The overall performance of the geometries investigated was evaluated using the thermal performance factor (TPF), which accounts for both heat transfer enhancement and pressure-drop penalty (Fig. 19). Among all cases, the deep-grooved pipe (case e) achieved the highest average TPF (≈1.43), indicating strong thermal enhancement relative to the smooth pipe. However, this improvement is accompanied by a substantially higher friction factor, leading to increased pumping power requirements and potentially higher operating costs. The remaining modified geometries show more balanced performance. The convex dimpled pipe (case b) yielded an average TPF of 0.95, with performance decreasing at higher Reynolds numbers due to pressure drop penalties. In contrast, the concave dimpled pipe (case c) and the shallow-grooved pipe (case d) achieved average TPF values of 1.12 and 1.24, respectively. These configurations provide meaningful heat transfer enhancement while maintaining moderate hydraulic losses. Overall, the results highlight the importance of selecting geometries that enhance heat transfer without incurring excessive pressure-drop penalties. Cases (c) and (d) offer the most favorable balance between thermal efficiency and pumping power.

Although the presented CFD results are for specific surface-modified geometry configurations and boundary conditions, the observed behavior of heat transfer enhancement is consistent with that reported in the literature. However, to generalize the presented CFD approach across different engineering conditions, it is recommended to conduct geometric parametric and experimental investigations for different fluids and operating conditions, such as varying wall heat flux. Moreover, it is worth noting that the presented study focuses on the thermal-hydraulic performance of surface-modified pipes, including heat transfer enhancement and pressure drop penalties. Definitely, they are directly related to pumping power and energy efficiency. However, the thermal performance factor shows the primary key indicator of the benefit of the surface-modified pipes under investigation. The operating expenses and the system's energy balance are beyond the scope of this work, which is a limitation and could be considered in future work.

4. Conclusion

This study investigates the thermal performance of dimpled and grooved heat pipes numerically using the CFD approach. The following are the main conclusions:

- The thermal performance factor for the pipe with convex dimples indicated no heat transfer enhancement compared to other investigated modified geometries.
- The pipe with concave dimples showed moderate thermal enhancement, exhibiting an average heat transfer increase of approximately 12% compared to the smooth pipe, with a reasonable increase in pressure drop.
- The grooved pipe with a groove depth-to-diameter ratio of 0.5 exhibited thermal enhancement by around 43%, which showed to be having the highest thermal enhancement compared to other configurations, but experiencing the highest-pressure penalty.
- The grooved pipe with a groove depth-to-diameter ratio of 0.2 exhibited a reasonable thermal enhancement by around 24%, and the average friction factor ratio relative to the smooth pipe was 3.4.

The investigation presented on surface-modified pipes provides a validated heat transfer enhancement technique and compares it with that of traditional smooth pipes. The study provides guidance on selecting the appropriate thermal enhancement technique, accounting for pressure drop penalties during the early design stage of heat pipes. However, further investigations are needed to generalize the presented CFD approach, including conducting a geometrical optimization study, extending the operating conditions, and exploring alternative working fluids. Future work will focus on integrating concave dimples with grooves into a heat pipe, and on investigating the effects of turbulence models and wall functions on thermal performance to improve the robustness of simulation outcomes.

Conflicts of interest

The authors declare no conflicts of interest.

Author contributions

Conceptualization, Mazen M. Othayq, and Khalid M. Alanazi; methodology, Mazen M. Othayq, and Khalid M. Alanazi; software, Mazen M. Othayq; validation, Mazen M. Othayq, and Khalid M. Alanazi; formal analysis, Mazen M. Othayq, and Khalid M. Alanazi; investigation, Mazen M. Othayq, and Khalid M. Alanazi; data curation, Mazen M. Othayq, and Khalid M. Alanazi; writing—original draft preparation, Mazen M. Othayq, and Khalid M. Alanazi; writing—review and editing, Mazen M. Othayq, and Khalid M. Alanazi.

Funding

This research received no external funding.

Data availability statement

The original contributions presented in this study are included in the article. Further inquiries can be directed to the authors.

References

1. Osintsev K, Aliukov S, Kuskarbekova S, Tarasova T, Karelin A, Konchakov V, Kornyakova O. Increasing Thermal Efficiency: Methods, Case Studies, and Integration of Heat Exchangers with Renewable Energy Sources and Heat Pumps for Desalination. Energies (Basel). 2023;16(13). https://doi.org/10.3390/en16134930.
2. Abraham JD, Dhoble AS, Mangrulkar CK. Numerical Analysis for Thermo-Hydraulic Performance of Staggered Cross Flow Tube Bank with Longitudinal Tapered Fins. International Communications in Heat and Mass Transfer. 2020;118. https://doi.org/https://doi.org/10.1016/j.icheatmasstransfer.2020.104905.
3. Mangrulkar C, Dhoble A, Abraham JD, Chamoli S. Experimental and Numerical Investigations for Effect of Longitudinal Splitter Plate Configuration for Thermal-Hydraulic Performance of Staggered Tube Bank. Int. J. Heat Mass Transf. 2020;161. https://doi.org/https://doi.org/10.1016/j.ijheatmasstransfer.2020.120280.
4. Mangrulkar CK, Dhoble AS, Chamoli S, Gupta A, Gawande VB. Recent Advancement in Heat Transfer and Fluid Flow Characteristics in Cross Flow Heat Exchangers. Renewable and Sustainable Energy Reviews. 2019;113(c):1–1. https://doi.org/https://doi.org/10.1016/j.rser.2019.06.027.
5. Mohammadi S, Mousavi Ajarostaghi SS, Pourfallah M. The Latent Heat Recovery from Boiler Exhaust Flue Gas Using Shell and Corrugated Tube Heat Exchanger: A Numerical Study. Heat Transfer. 2020;49(6):3797–3815. https://doi.org/https://doi.org/10.1002/htj.21809.
6. Zheng N, Liu W, Liu Z, Liu P, Shan F. A Numerical Study on Heat Transfer Enhancement and the Flow Structure in a Heat Exchanger Tube with Discrete Double Inclined Ribs. Appl. Therm. Eng. 2015;90:232–241. https://doi.org/10.1016/J.APPLTHERMALENG.2015.07.009.
7. Chang SW, Chiang KF, Chou TC. Heat Transfer and Pressure Drop in Hexagonal Ducts with Surface Dimples. Exp. Therm. Fluid Sci. 2010;34(8):1172–1181. https://doi.org/10.1016/J.EXPTHERMFLUSCI.2010.04.006.
8. Li M, Khan TS, Al Hajri E, Ayub ZH. Geometric Optimization for Thermal–Hydraulic Performance of Dimpled Enhanced Tubes for Single Phase Flow. Appl. Therm. Eng. 2016;103:639–650. https://doi.org/10.1016/J.APPLTHERMALENG.2016.04.141.
9. Xie S, Liang Z, Zhang J, Zhang L, Wang Y, Ding H. Numerical Investigation on Flow and Heat Transfer in Dimpled Tube with Teardrop Dimples. Int. J. Heat Mass Transf. 2019;131:713–723. https://doi.org/10.1016/J.IJHEATMASSTRANSFER.2018.11.112.
10. Xie S, Liang Z, Zhang L, Wang Y. A Numerical Study on Heat Transfer Enhancement and Flow Structure in Enhanced Tube with Cross Ellipsoidal Dimples. Int. J. Heat

Mass Transf. 2018;125:434–444. https://doi.org/10.1016/J.IJHEATMASSTRANSFER.2018.04.106.
11. Ali MA, Shehab SN. Hydrothermal Characteristics of Water Flow into a Dimpled Tube Heat Exchanger: A Parametric Study. Frontiers in Heat and Mass Transfer 2022;19. https://doi.org/10.5098/hmt.19.39.
12. Gürdal M, Pazarlıoğlu HK, Tekir M, Arslan K, Gedik E. Numerical Investigation on Turbulent Flow and Heat Transfer Characteristics of Ferro-Nanofluid Flowing in Dimpled Tube under Magnetic Field Effect. Appl. Therm. Eng. 2022;200:117655. https://doi.org/10.1016/J.APPLTHERMALENG.2021.117655.
13. Falih AH, Khalaf BS, Freegah B. Investigate the Impact of Dimple Size and Distribution on the Hydrothermal Performance of Dimpled Heat Exchanger Tubes. Frontiers in Heat and Mass Transfer. 2024;22(2):597–613. https://doi.org/10.32604/fhmt.2024.049812.
14. Ahmed Ali S, Barrak ES, Alrikaby NJ, Hameed MR. Numerical Study of Thermal-Hydraulic Performance of Forced Convection Heat Transfer in Dimple Surface Pipe with Different Shapes Using Commercial CFD Code. Journal of Advanced Research in Fluid Mechanics and Thermal Sciences. 2025;125(2):1–15. https://doi.org/10.37934/arfmts.125.2.115.
15. AL-OBAIDI AR, ALHAMID J. Influence of Different Geometrical Dimple Configurations on Flow Behaviour and Thermal Performance within a 3D Circular Pipe. Journal of Thermal Engineering. 2024;10(1):175–187. https://doi.org/10.18186/thermal.1429903.
16. Malapur HV, Havaldar SN, Kharade UV. Heat Transfer Enhancement of an Internally and Externally Dimpled Pipe Heat Exchanger – Numerical Study. Materials Today: Proceedings, Elsevier Ltd. 2022;587–594. https://doi.org/10.1016/j.matpr.2022.04.155.
17. Ying P, He Y, Tang H, Ren Y. Numerical and Experimental Investigation of Flow and Heat Transfer in Heat Exchanger Channels with Different Dimples Geometries. Machines. 2021;9(4). https://doi.org/10.3390/machines9040072.
18. Al-Obaidi AR, Chaer I. Flow Field Structure, Characteristics of Thermo-Hydraulic and Heat Transfer Performance Analysis in a Three Dimensions Circular Tube with Different Ball Turbulators Configurations. Arab. J. Sci. Eng. 2021;46(12):12253–12282. https://doi.org/10.1007/s13369-021-05943-7.
19. Li M, Khan TS, Al-Hajri E, Ayub ZH. Single Phase Heat Transfer and Pressure Drop Analysis of a Dimpled Enhanced Tube. Appl. Therm. Eng. 2016;101:38–46. https://doi.org/10.1016/J.APPLTHERMALENG.2016.03.042.
20. Ali SA. Using Ansys Fluent to Study Flow Characteristics and Heat Transfer Enhancement by Inserting Different Sizes of Dimple in Three-Dimensional Horizontal Single Pipe Heat Exchanger. Journal of Advanced Industrial Technology and Application. 2025.
21. Dagdevir T, Ozceyhan V. An Experimental Study on Heat Transfer Enhancement and Flow Characteristics of a Tube with Plain, Perforated and Dimpled Twisted Tape Inserts. International Journal of Thermal Sciences. 2021;159. https://doi.org/https://doi.org/10.1016/j.ijthermalsci.2020.106564.
22. Zhang L, Xiong W, Zheng J, Liang Z, Xie S. Numerical Analysis of Heat Transfer Enhancement and Flow Characteristics inside Cross-Combined Ellipsoidal Dimple Tubes. Case Studies in Thermal Engineering. 2021;25. https://doi.org/10.1016/j.csite.2021.100937.
23. Zhou F, Acharya S. Experimental and Computational Study of Heat/Mass Transfer and Flow Structure for Four Dimple Shapes in a Square Internal Passage. ASME Turbo Expo 2009: Power for Land, Sea, and Air, The American Society of Mechanical Engineers. 2010;939–953. https://doi.org/https://sci-hub.st/10.1115/GT2009-60240.
24. Pandit J, Thompson M, Ekkad SV, Huxtable ST. Effect of Pin Fin to Channel Height Ratio and Pin Fin Geometry on Heat Transfer Performance for Flow in Rectangular Channels. Int. J. Heat Mass Transf. 2014;77:359–368. https://doi.org/10.1016/J.IJHEATMASSTRANSFER.2014.05.030.
25. Xie G, Liu J, Ligrani PM, Zhang W. Numerical Predictions of Heat Transfer and Flow Structure in a Square Cross-Section Channel with Various Non-Spherical Indentation Dimples. An International Journal of Computation and Methodology. 2013;64(3):187–215. https://doi.org/https://doi.org/10.1080/10407782.2013.779485.
26. Li M, Khan TS, Hajri EA, Ayub ZH. Geometric Optimization for Thermal-Hydraulic Performance of Dimpled Enhanced Tubes for Single Phase Flow. Appl. Therm. Eng. 2016;103:639–650. https://doi.org/https://doi.org/10.1016/j.applthermaleng.2016.04.141.
27. Xie S, Liang Z, Zhang L, Wang Y, Ding H, Zhang J. Numerical Investigation on Heat Transfer Performance and Flow Characteristics in Enhanced Tube with Dimples and Protrusions. Int. J. Heat Mass Transf. 2018;122:602–613. https://doi.org/10.1016/j.ijheatmasstransfer.2018.01.106.
28. Naphon P, Nuchjapo M, Kurujareon J. Tube Side Heat Transfer Coefficient and Friction Factor Characteristics of Horizontal Tubes with Helical Rib. Energy Convers. Manag. 2006;47(18–19):3031–3044. https://doi.org/10.1016/J.ENCONMAN.2006.03.023.
29. Laohalertdecha S, Wongwises S. The Effects of Corrugation Pitch on the Condensation Heat Transfer Coefficient and Pressure Drop of R-134a inside Horizontal Corrugated Tube. Int. J. Heat Mass Transf. 2010;53(13–14):2924–2931. https://doi.org/10.1016/J.IJHEATMASSTRANSFER.2010.01.037.
30. Pethkool S, Eiamsa-ard S, Kwankaomeng S, Promvonge P. Turbulent Heat Transfer Enhancement in a Heat Exchanger Using Helically Corrugated Tube. International Communications in Heat and Mass Transfer. 2011;38(3):340–347. https://doi.org/10.1016/J.ICHEATMASSTRANSFER.2010.11.014.
31. Elshafei EAM, Awad MM, El-Negiry E, Ali AG. Heat Transfer and Pressure Drop in Corrugated Channels. Energy. 2010;35(1):101–110. https://doi.org/10.1016/J.ENERGY.2009.08.031.
32. Dong Y, Huixiong L, Tingkuan C. Pressure Drop, Heat Transfer and Performance of Single-Phase Turbulent Flow in Spirally Corrugated Tubes. Exp. Therm. Fluid Sci. 2001;24(3–4):131–138. https://doi.org/10.1016/S0894-1777(01)00047-4.
33. Talib RN, Yasin NJ, Nasser MA. The Effect of External Helical Ribs Tube on the Heat Transfer and Pressure Drop Performance for Multi - Tube Heat Exchanger. IOP Conference Series: Materials Science and Engineering, Institute of Physics Publishing. 2019. https://doi.org/10.1088/1757-899X/518/3/032015.
34. Leontiev AI, Kiselev NA, Burtsev SA, Strongin MM, Vinogradov YA. Experimental Investigation of Heat Transfer and Drag on Surfaces with Spherical Dimples. Exp. Therm. Fluid Sci. 2016;79:74–84. https://doi.org/10.1016/J.EXPTHERMFLUSCI.2016.06.024.
35. Jackson JD, Büyükalaca O, He S. Heat Transfer in a Pipe under Conditions of Transient Turbulent Flow. Int. J. Heat Fluid Flow 1999;20(2):115–127. https://doi.org/10.1016/S0142-727X(98)10056-5.
36. Du W, Luo L, Wang S, Zhang X. Heat Transfer Characteristics in a Pin Finned Channel With Different Dimple Locations.

Heat Transfer Engineering. 2020;41(14):1231–1251. https://doi.org/https://doi.org/10.1080/01457632.2019.1637114.
37. Fan JF, Ding WK, He YL, Tao WQ. Three-Dimensional Numerical Study of Fluid and Heat Transfer Characteristics of Dimpled Fin Surfaces. 2012;62(4):271–294. https://doi.org/https://doi.org/10.1080/10407782.2012.666931?urlappend=%3Futm_source%3Dresearchgate.net%26utm_medium%3Darticle.
38. Katkhaw N, Vorayos N, Kiatsiriroat T, Khunatorn Y, Bunturat D, Nuntaphan A. Heat Transfer Behavior of Flat Plate Having 45° Ellipsoidal Dimpled Surfaces. Case Studies in Thermal Engineering. 2014;2:67–74. https://doi.org/https://doi.org/10.1016/j.icheatmasstransfer.2020.104905.
39. Piper M, Zibart A, Djakow E, Springer R, Homberg W, Kenig EY. Heat Transfer Enhancement in Pillow-Plate Heat Exchangers with Dimpled Surfaces: A Numerical Study. Appl. Therm. Eng. 2019;153:142–146. https://doi.org/10.1016/J.APPLTHERMALENG.2019.02.082.
40. Farsad S, Mashayekhi M, Zolfagharnasab MH, Lakhi M, Farhani F, Zareinia K, Okati V. The Effects of Tube Dimples-Protrusions on the Thermo-Fluidic Properties of Turbulent Forced-Convection. Case Studies in Thermal Engineering. 2022;35. https://doi.org/10.1016/j.csite.2022.102033.
41. Al-Haidari SR, Al-Obaidi AR, Saleh ZM, Mohammed A, Ismail HB. Enhancement of Thermohydraulic Performance in 3D Pipe Based on Different Concavity Dimpled Surfaces: Numerical and Experimental Investigation. Case Studies in Thermal Engineering. 2025;75:107153. https://doi.org/10.1016/j.csite.2025.107153.
42. Mashayekh K, Etminan A, Pope K, Muzychka YS. Hydrothermal Performance of Turbulent Flow in Tubes with Spherical Dimples. International Journal of Thermal Sciences. 2025;215:110027. https://doi.org/10.1016/j.ijthermalsci.2025.110027.
43. “ANSYS Fluent User’ s Guide.”
44. Vijiapurapu S, Cui J. Performance of Turbulence Models for Flows through Rough Pipes. Appl. Math. Model. 2010;34(6):1458–1466. https://doi.org/10.1016/j.apm.2009.08.029.
45. Mei S, Qi C, Luo T, Zhai X, Yan Y. Effects of Magnetic Field on Thermo-Hydraulic Performance of Fe3O4-Water Nanofluids in a Corrugated Tube. Int. J. Heat Mass Transf. 2019;128:24–45. https://doi.org/10.1016/j.ijheatmasstransfer.2018.08.071.
46. Gnielinski V. New Equations for Heat and Mass Transfer in Turbulent Pipe and Channel Flow. Journal of Engineering Physics. 1976. https://doi.org/https://api.semanticscholar.org/CorpusID:136639967.
47. Lu H, Wang Y, Li H, Zhao W. Numerical Simulation of Turbulent Structure and Particle Deposition in a Three-Dimensional Heat Transfer Pipe with Corrugation. Energies. 2024;17:321. https://doi.org/10.3390/en17020321.
48. He S. On Transient Turbulent Pipe Flow. University of Manchester. 1992.